Materials & Design 264 (2026) 115704

Contents lists available at ScienceDirect

Materials & Design

journal homepage: www.elsevier.com/locate/matdes

Pellet-fed continuous-silk-fibre 3D/4D printing of PLA/bamboo-charcoal bio-composites with shape recovery and thermomechanical stability

Kaveh Rahmani [a], Shawn Ravanbod [a], Mohammadreza L. Dezaki [a], Callum Branfoot [b], Mahdi Bodaghi [a,*]

[a] Department of Engineering, School of Science and Technology, Nottingham Trent University, Nottingham NG11 8NS, UK
[b] Engineering Operations, National Composites Centre, Bristol BS16 7FS, UK

ARTICLE INFO

Keywords:
Fused granulate fabrication
3D/4D printing
Natural continuous fibres
PLA composites
Metamaterials

ABSTRACT

A pellet-fed extrusion platform with integrated continuous-fibre co-deposition is presented, enabling 3D/4D printing of bio-composites directly from pellets, avoiding a separate filament-making step, thereby reducing time, energy, and material waste. A polylactic acid/bamboo-charcoal/continuous-silk-fibre (PLA/BC/CSF) system was formulated to overcome PLA's low strength, thermal creep, and flammability. With 3 wt% BC, PLA tensile strength increased by 28%; with CSF, tensile strength reached 108 MPa (+213% vs PLA). Three-point bending strength rose + 247% over PLA (+200% vs PLA/BC; +40% vs PLA/CSF). The burning rate decreased by 41% relative to PLA, evidencing improved flame resistance. Under 70 °C and constant load, PLA/BC/CSF beams retained geometry whereas PLA sagged, confirming superior thermo-mechanical stability. Architected honeycomb and trapezium meta-composites printed from PLA/BC/CSF exhibited quasi-constant force, and quasi-zero stiffness plateaus with energy dissipation and shape recovery (full after 25% compression; 85% recovery after 45% upon heat activation), supporting reuse and overload protection. The approach delivers a low-cost, lower-energy route to continuous-fibre bio-composites and demonstrates printable, recoverable components for logistics and automotive use (e.g., pallets, chassis inserts, dashboard face-parts), advancing sustainable additive manufacturing and circular-economy goals.

1. Introduction

3D printing technologies, particularly fused filament fabrication (FFF), have emerged as transformative platforms for manufacturing advanced composite materials. Conventional 3D-printed polymers and short fibre-reinforced composites often demonstrate relatively modest mechanical performance due to inherent process-induced defects such as porosity, weak interfacial adhesion, and low fibre content. In contrast, continuous fibre-reinforced composites (CFRCs) exhibit significantly superior mechanical properties, including enhanced tensile strength, stiffness, and fatigue resistance, making them promising candidates for load-bearing and structural applications [1,2]. Their adoption across various engineering sectors, including automotive and aerospace industries, has been bolstered by their high strength-to-weight and stiffness-to-weight ratios, along with controllable fibre orientation and architecture [3,4].

The development of low-cost and versatile manufacturing routes has historically been central to the evolution and widespread adoption of composites. In this context, the advent of 3D and 4D printing has opened up unique opportunities to expand the design flexibility and functionality of composite materials [5–8]. Among the additive manufacturing processes, FFF has become one of the most widely investigated techniques for fabricating CFRCs due to its relatively low cost, process simplicity, and compatibility with a wide range of thermoplastic matrices. However, building upon decades of experience in conventional composite fabrication, most studies to date have remained focused on the 3D/4D printing of synthetic CFRCs, such as carbon- or glass-fibre reinforced polymers [9–11]. Despite their promising structural performance, several limitations inherent to synthetic CFRCs produced via FFF have been consistently reported. These drawbacks include restricted material availability, inadequate inter-filament bonding, anisotropy-induced performance degradation, and, importantly, the environmental burden associated with the production and disposal of petroleum-derived fibres and matrices [12–14]. With growing global

* Corresponding author.
E-mail address: mahdi.bodaghi@ntu.ac.uk (M. Bodaghi).

https://doi.org/10.1016/j.matdes.2026.115704
Received 30 October 2025; Received in revised form 22 January 2026; Accepted 20 February 2026
Available online 21 February 2026

emphasis on sustainable development and the protection of natural ecosystems, these shortcomings render synthetic CFRCs increasingly incompatible with the imperatives of environmentally responsible manufacturing. Consequently, there is an urgent need to integrate environmental considerations into the development of next-generation composite materials.

The integration of natural fillers and fibres into polymer matrices presents a promising pathway toward the development of greener, biodegradable, and lower-impact composites. The benefits of these materials arise not only from their abundant availability and renewability but also from their potential to enhance biodegradability and reduce the life-cycle carbon footprint of the resulting structures. Recent studies have shown that FFF-based 3D/4D printing can be rendered more sustainable through the use of natural continuous fibre-reinforced composites (CFRCs), while improving mechanical/material characteristics [15–21]. To name a few works, Lalegani Dezaki et al. [15] developed bio-based gradient composites for 3D/4D printing, which exhibited enhanced mechanical, shape memory, and flame-retardant properties. Such bio-based composites can change their properties in response to external or internal triggers, enabling potential applications in targeted biomedical fields [22]. Bodaghi et al. [19] proposed a bio-composite by incorporating polylactic acid (PLA) with bamboo charcoal (BC) and printed it using a modified printer equipped with a dual-feed system to accommodate both PLA/BC filaments and continuous flax fibres. This approach improved tensile strength by 248% and flexural strength by 207%. Khan et al. [20] investigated the physical, mechanical, and thermal properties of bamboo and kenaf (KF) fibre-reinforced PLA hybrid composites. The bamboo-PLA non-hybrid composite exhibited the highest tensile strength at 25.95 MPa and compressive strength at 173.15 MPa, while the 30bamboo-70KF hybrid composite showed notable impact strength.

Among the various natural resources, BC has garnered significant interest due to its advantageous properties, including high mechanical strength and rapid renewability [23]. BC can be incorporated into polymer composites in various forms, long fibres, short fibres, or powders, each offering distinct reinforcement mechanisms within the polymer matrix. Rahmani et al. [24] indicated that BC particles not only enhance mechanical performance but also improve flame retardancy. Similarly, other natural reinforcements, such as eggshell (EGS) powders [25], chitosan particles [26], and protein-based fibres (e.g., silk) [27], have proven capable of significantly strengthening polymer matrices and customising their functional properties. Silk, in particular, stands out as a highly promising bio-based reinforcement owing to its unique combination of mechanical robustness and biocompatibility. Primarily composed of fibroin, silk is produced by the larvae of Bombyx species and has found extensive application in biomedical additive manufacturing. In the context of 3D/4D printing, silk has primarily been utilised in bioinks for hydrogel-based scaffolds designed for tissue regeneration [28]. Its incorporation into thermoplastic matrices has been shown to markedly enhance both biological and mechanical properties [29,30]. For instance, Vyas et al. [31] showed that the integration of silk microparticles into polycaprolactone matrices at concentrations of up to 20% significantly improves compressive strength and modulus. This underscores the potential of silk fibres as effective continuous reinforcements in structural polymer composites.

Despite rapid progress in 3D/4D printing of PLA composites, all studies have centred on synthetic or natural CFRCs produced by FFF, where limited material choice, sub-optimal fibre impregnation, and the environmental burden of petro-derived constituents and filament making remain drawbacks. Parallel work on bio-based reinforcements shows promise, e.g., BC particulates for strength/flame retardancy and protein fibres such as silk for toughness, yet their continuous-fibre integration and/or pellet-based processing have been unexplored. To address these gaps, a pellet-fed extrusion 3D printing platform is introduced as a class of fused granulate fabrication (FGF) integrated with continuous-fibre co-deposition. It prints directly from pellets, eliminating filament making and improving fibre wet-out, deposition speed, and structural integrity. A bio-composite with PLA matrix reinforced with BC at micro level and continuous silk fibres (CSF) at macro level is formulated. Its performance is systematically evaluated via tension, bending, dynamic thermomechanical analysis (DMA), flammability, thermo-mechanical stability, and shape-memory under cold/hot programming. Architected honeycomb and trapezium meta-composites are then demonstrated, exploiting quasi-zero-stiffness and quasi-constant force plateaus for energy dissipation/over-load protection and heat-activated shape recovery for reuse. The contributions are: (a) a low-energy, filament-free route for continuous-fibre bio-composites; (b) a validated PLA/BC/CSF system combining strength, flame resistance, and high-temperature stability; and (c) functionally recoverable meta-composites with application paths in logistics and automotive structures aligned with circular-economy principles.

2. Materials

This section provides a comprehensive overview of the constituent materials utilised in the fabrication of the proposed fibre-reinforced bio-composite. Specifically, it introduces PLA as the polymer matrix, alongside BC and silk fibres, which serve as natural reinforcements. Their material characteristics, such as biodegradability, mechanical performance, and compatibility within sustainable composite systems are evaluated. Fig. 1 demonstrates the bio-composite feedstocks used in the composite development process.

2.1. Polylactic acid

Semi-crystalline PLA (NatureWorks 4043D) pellets with a diameter of 3–4 *mm*, supplied by RESINEX Company, were employed as the polymeric matrix. PLA is an eco-friendly thermoplastic polymer derived from renewable resources and exhibits shape memory effect (SME) characteristics (Fig. 1(I)). Owing to its ability to recover pre-defined shapes, PLA has found extensive applications in advanced manufacturing processes such as 3D/4D printing. The material possesses a melting range of 150–165 °C, a glass transition temperature Tg of 55–65 °C, and a reported melting temperature of approximately 200 °C [32].

2.2. Bamboo charcoal powder

BC particles, with particle size of approximately 25 μ*m* from a natural plant resource obtained from Takesumi Ltd. (Japan), were incorporated as reinforcement to enhance the structural strength and flame-retardant properties of the PLA matrix (Fig. 1(II)). The integration of natural and biodegradable fillers such as BC aligns with the growing emphasis on sustainable composite development [23,33]. Derived from bamboo, BC is an abundant, renewable, cost-effective, non-toxic, and chemically stable material. Owing to these properties, it has been widely utilised across diverse fields, including engineering, food processing, cosmetics, pharmaceuticals, and healthcare [34].

2.3. Continuous silk fibre

Continuous silk fibres sourced from a textile manufacturer, were employed as reinforcement to provide superior tensile strength and enhance structural integrity (Fig. 1(III)). CSF is one of the oldest and most extensively used bio-fibres, historically applied in extraction, spinning, and textile production. Due to their outstanding tensile performance, silk fibres are recognised as among the most effective natural reinforcements for polymer composites. The silk yarn utilised in this study consisted of fine unwaxed natural linen with a linear density of 38 Tex × 2, and 0.25 *mm* diameter.

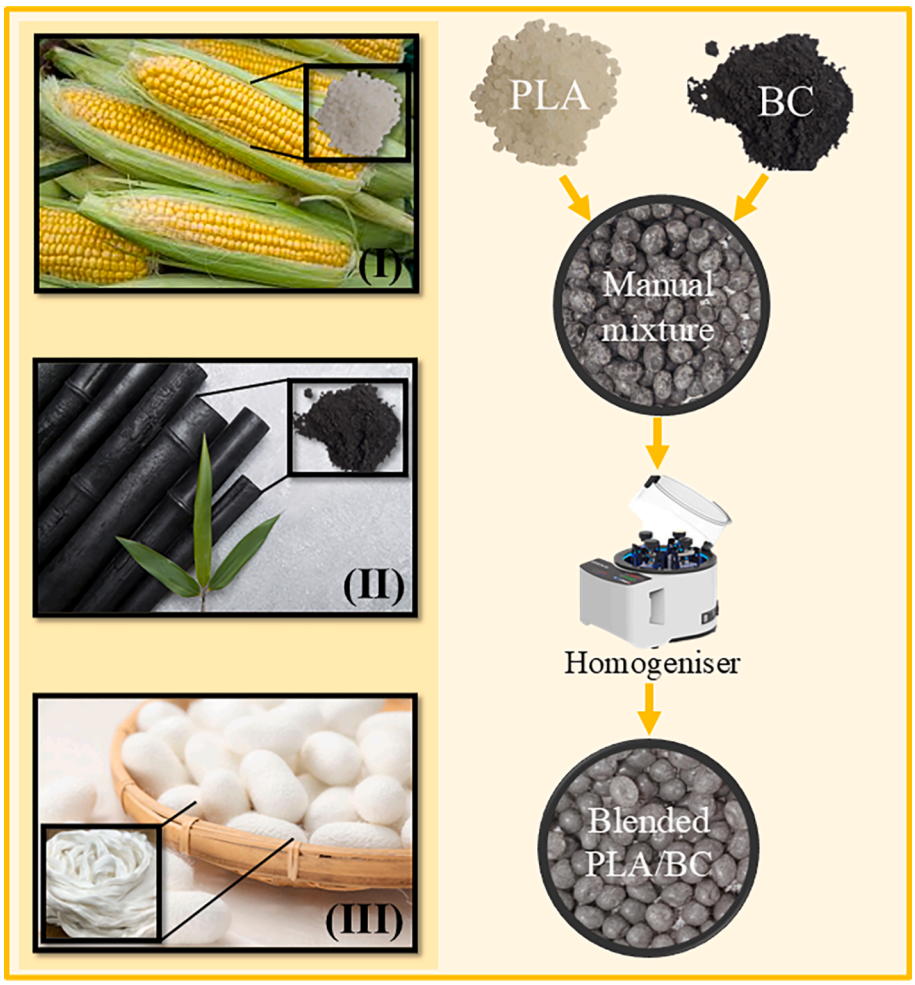

Fig. 1. Illustration of bio-composite feedstocks and the pellet reinforcement process. (I-III) show the feedstocks of PLA, BC, and silk, respectively.

3. Manufacturing and methods

This section provides a comprehensive overview of the manufacturing procedures employed for material extrusion and sample fabrication. To facilitate this process, a novel pellet-fed extrusion 3D printer (FGF class) was modified, specifically engineered to integrate continuous fibre reinforcement during printing. The design and implementation of this custom-built system address the limitations of conventional filament-based additive manufacturing by allowing the direct use of thermoplastic pellets, thereby enabling greater material versatility and cost efficiency. The incorporation of continuous fibre printing further enhances the mechanical performance of printed components by embedding high-strength fibres in situ during the extrusion process. Detailed descriptions of the printer configuration, material preparation, and operational parameters are presented to ensure reproducibility and to highlight the innovations introduced in the system.

3.1. Extrusion and printing process development

Both PLA pellets and BC particles exhibit hydrophobic characteristics yet remain susceptible to moisture absorption. Accordingly, the materials were pre-conditioned by mixing and subsequently dried in a hot-air dryer at 70 °C for 24h before extrusion. BC particles were incorporated into PLA at concentrations of 0, 1.5, 3, and 5 wt%. The BC content was defined based on weight fraction, and the corresponding volume fractions were calculated using the density of BC powder (0.415 g/cm^3) and PLA (1.24 g/cm^3). The calculated volume fractions of BC were approximately 4.4, 8.6, and 13.8 vol% for 1.5, 3, and 5 wt% BC, respectively. The mixtures were subsequently subjected to planetary ball milling as a solid-state dry mixing step, which de-agglomerates the BC particles and promotes their uniform distribution on the surface of the PLA pellets. It should be noted that no melting occurred during milling. Finally, the processed mixtures were then utilised as feedstock for FGF. Although the pellet-fed extrusion unit is relatively heavy and moves along the Z-axis, stable layer deposition was achieved by employing a screw-driven extrusion mechanism, a multi-zone heated process, and relatively low printing speeds (See Fig. 2). This configuration ensured a stable and homogeneous melt flow at the nozzle exit and enabled consistent layer control during FGF printing.

For the fabrication of polymer composites reinforced with CSF, a modified FGF pellet-fed extrusion system (PioCreat G5Ultra) was employed as illustrated in Fig. 3. The modification consisted of an additional feeding channel designed to introduce CSF directly into the extrusion pathway, thereby enabling the co-deposition of extruded PLA/BC composite filament and CSF at a single-output nozzle. To clarify the printing strategy and ensure reproducibility of the samples, slicer-generated schematics are provided, showing the toolpath, infill pattern, and a cross-sectional view of the layers (Fig. 4). These illustrations demonstrate the relationship between the feature size, layer height, and the overall design, making the fabrication process transparent and easy to interpret.

It is worth noting that the CSF was introduced into the extrusion head through a side-fed inlet located near the nozzle exit. The fibre feeder hole was designed with a diameter marginally larger than the fibre bundle, ensuring that the inlet remained effectively occupied during printing. This configuration prevents molten polymer from

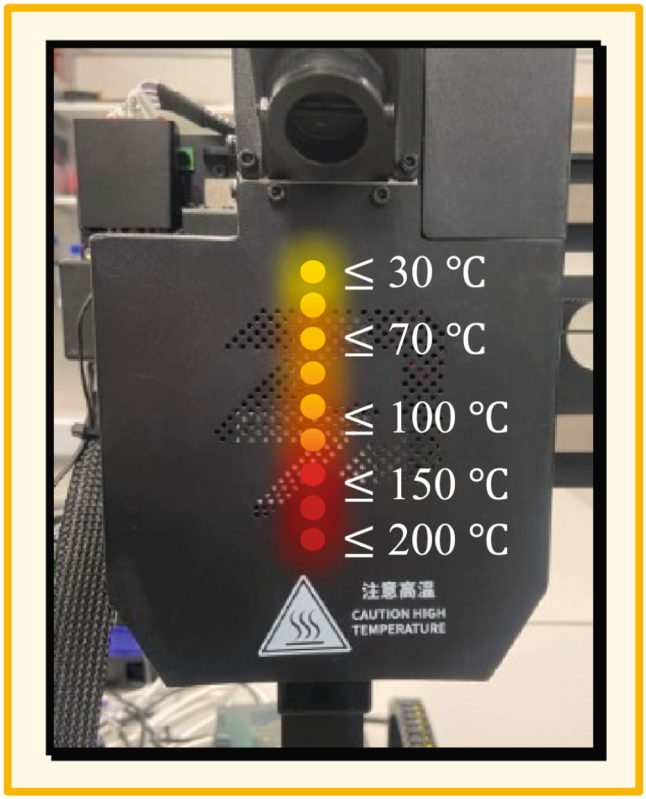

Fig. 2. Illustration of the pellet extruder featuring multi-zone segmented heating process for better thermal management.

escaping through the fibre inlet. Moreover, the internal pressure gradient within the nozzle is directed toward the main extrusion orifice, while the relatively high viscosity of the PLA/BC melt further suppresses backflow. This design enables stable fibre impregnation and co-deposition without melt leakage, consistent with previously reported continuous fibre additive manufacturing systems [35,36]. Also, the modified nozzle did not incorporate a fibre cutting mechanism; therefore, the CSF was deposited without interruption during printing. To accommodate this configuration, printing paths were designed as continuous tool paths without retraction or non-printing travel moves. Layer stacking was performed in a unidirectional, layer-by-layer pattern to preserve fibre continuity. All samples were fabricated under fixed processing parameters using a 1.8 *mm* nozzle, with no evidence of clogging observed. This nozzle size was chosen in the modified FFF printer to ensure smooth extrusion of the PLA/BC/CSF composite filaments, considering the presence of fillers and fibre reinforcements, following previous works on continuous fibre-reinforced composites where nozzle diameter was adapted to achieve reliable printing [37,38]. For clarity, samples composed solely of PLA/BC composites are denoted as PLA/BC, whereas those reinforced with CSF are designated as PLA/BC/CSF or PLA/CSF. Table 1 summarises the values selected for 3D printing.

4. Experimental setup

This section details the experimental setup and procedures implemented to systematically investigate the mechanical, thermo-mechanical, and fire-resistant properties of the fabricated samples. In addition, the experimental framework includes the characterisation of microstructural features and the evaluation of shape memory behaviour. A combination of standardised testing methods and advanced analytical techniques was employed to ensure accurate, reliable, and reproducible results across all evaluated properties. This comprehensive approach provides a robust foundation for understanding the performance and multifunctionality of the developed materials.

4.1. Mechanical and thermo-mechanical tests

The mechanical characterisation of the fabricated samples was conducted using a Shimadzu AG-X Plus universal testing machine, employing both tensile and three-point bending test configurations. Tensile tests were performed on four material groups: pure PLA, PLA/BC, PLA/BC/CSF, and PLA/CSF samples. These tests were carried out in accordance with ASTM D638 [39] and ASTM D3039 [40] standards. A crosshead speed of 5 *mm/min* was employed, with a grip separation

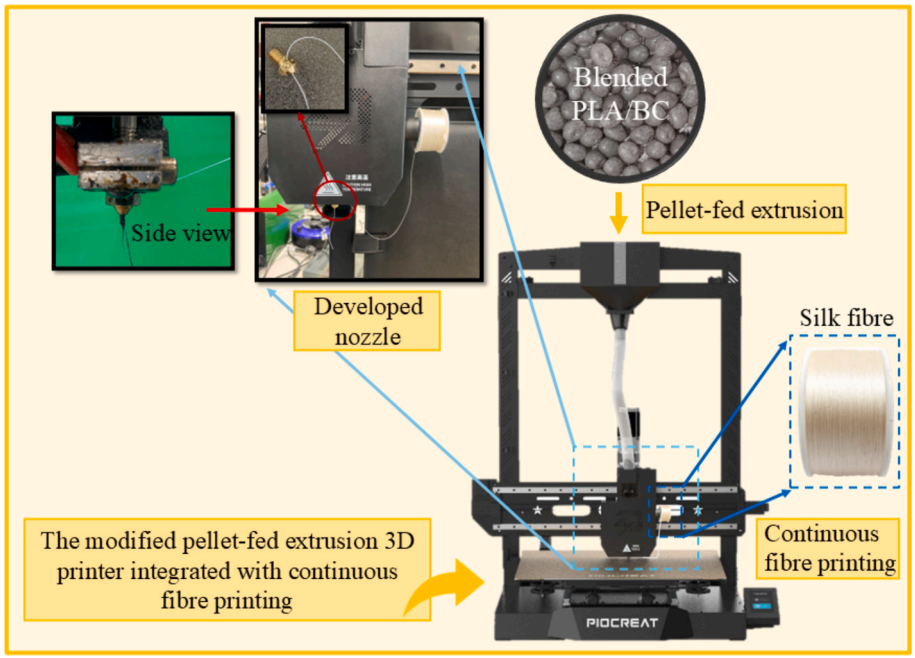

Fig. 3. Schematic presentation of the developed FGF platform integrated with continuous fibre feed.

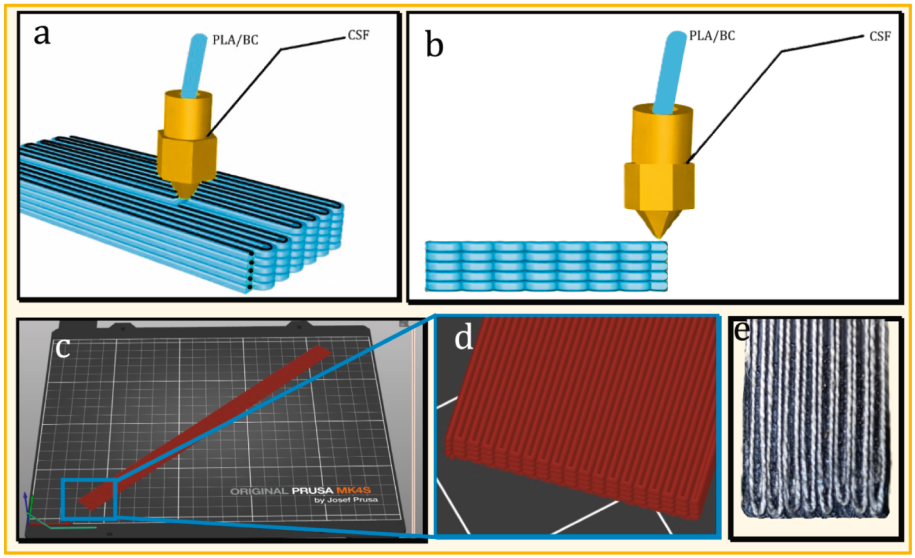

Fig. 4. Images of schematics, the toolpath, and the infill pattern (a) isometric view, (b) a cross-sectional view of the layers, (c) slicer-generated, (d) high magnification of slicer-generated, and (e) the printed sample.

Table 1
Printing parameters set in the fabrication process.

Parameters	Value
Nozzle temperature (°C)	200
Bed temperature (°C)	60
Infill density (%)	100
Nozzle diameter (*mm*)	1.8
Layer thickness (*mm*)	0.2
Printing speed (*mm/s*)	30

distance of 100 *mm*. During testing, the bottom grip remained stationary while the upper grip was displaced vertically to apply a tensile load. Three-point bending tests were conducted in accordance with the ASTM D790 [41] standard, using a support span of 50 *mm* and a loading speed of 5 *mm/min*. The calculation of stress and strain is based on ASTM D790 as follows:

$$\sigma_{3PB} = \frac{3FL}{2bd^2} \tag{1}$$

$$\epsilon_{3PB} = \frac{6Dd}{L^2} \tag{2}$$

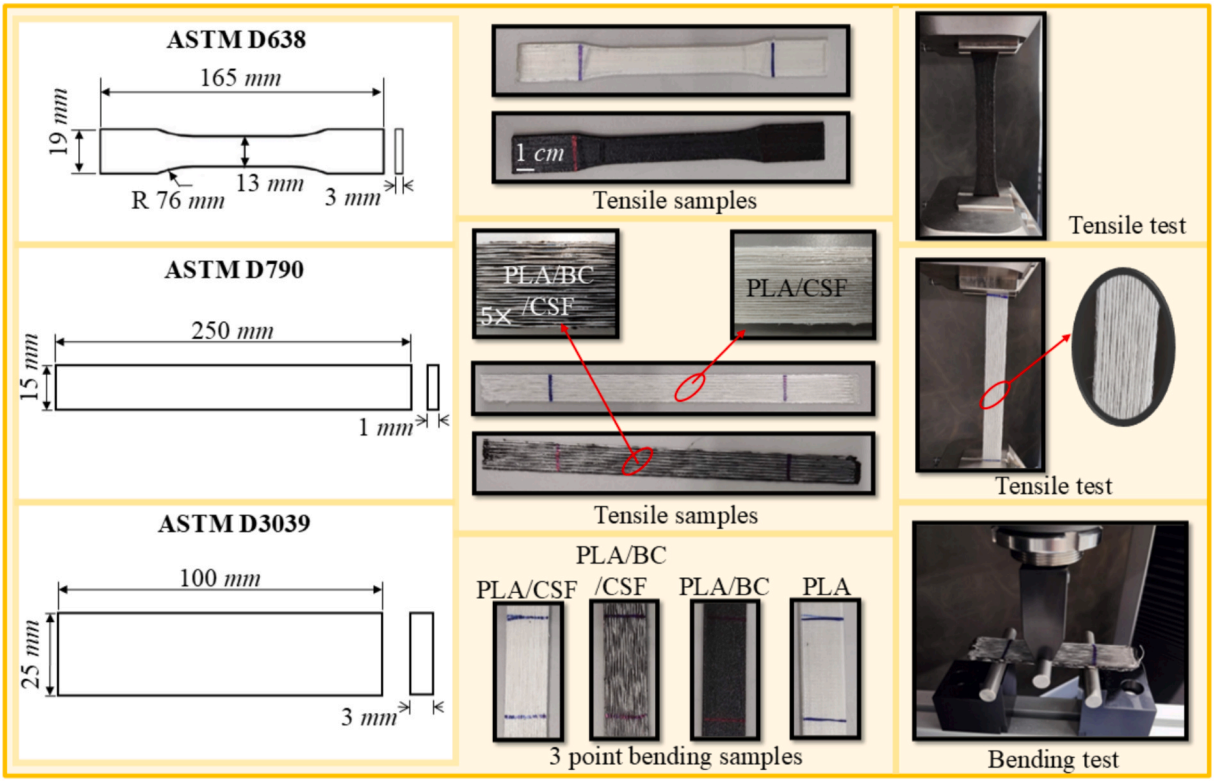

Fig. 5. Illustration of fabricated ASTM dog-bone specimens along with dimensions. Experimental setups for tensile and three-point bending tests are also presented.

In this context, F represents the force causing bending, L denotes the distance between supports, b stands for the width of the test sample, d represents its thickness, and D is the maximum deflection of the centre of the beam.

All mechanical tests were performed under standard laboratory conditions. For each material group, five replicate specimens were tested, and the mean values of the measured parameters were reported to ensure statistical reliability. To maximise anisotropic strength characteristics, all specimens were 3D-printed in the longitudinal direction, aligning the principal printing axis with the direction of the applied mechanical load. Fig. 5 presents the 2D schematic drawings of the test specimens designed in accordance with the relevant ASTM standards, along with images of the 3D-printed dog-bones and the corresponding mechanical test setups.

The SME of the 3D-printed bio-composites is fundamentally governed by key thermomechanical parameters: the storage modulus (E') and the glass transition temperature Tg and the damping factor (tan δ). Tan δ, defined as the ratio of the loss modulus to the storage modulus, reflects the viscoelastic energy dissipation and molecular mobility within the polymer matrix and is commonly used to identify relaxation behaviour associated with Tg. In the context of SME, tan δ provides important insight into the balance between elastic energy storage and viscous dissipation, which directly influences shape fixation and recovery performance. In this study, particular attention was given to evaluating the influence of natural fibre reinforcements and BC particles on the SME behaviour of semi-crystalline PLA matrices. To this end, DMA was performed using a PerkinElmer DMA 8000 instrument as shown in Fig. 6. The analysis was conducted on both pure PLA and PLA/BC/CSF composite samples. Test specimens were fabricated with dimensions of 30 *mm* in length, 8 *mm* in width, and 1 *mm* in thickness. The temperature range for the DMA tests spanned from 20 °C to 80 °C, using a heating rate of 5°C/min and a frequency of 1 Hz under a tension load in dual cantilever mode, where the load was applied along the sample length, aligned with the fibre direction. This testing protocol enabled precise evaluation of the material's viscoelastic response and facilitated the assessment of its mechanical potential under thermomechanical stimuli.

4.2. Microstructure examination

A scanning electron microscope (SEM) model JSM-7100F LV FEG was utilised to assess the microstructure, fracture surfaces, and fibre distribution in the printed samples. Prior to imaging, a thin gold coating was applied to the samples for better image clarity.

4.3. Flame-resistance test

The flammability of the samples was assessed in accordance with ASTM D635–22 and ASTM D3801, respectively, to measure the burning rate and durationin a horizontal position and limiting oxygen index (LOI)measurements, and cone calorimeter tests (CCTs) in a vertical position [42]. Printed strips were arranged in a smoke hood and marked at 25 *mm* and 100 *mm* from one end. One end of each strip was subjected to a heated gas burner until the flame penetrated 6 *mm*, at which point timing commenced. The duration for the flame to travel between the two markings was recorded, and the burning rate was then calculated using the following equation.

$$V = (60 \times L)/t, \tag{3}$$

where V represents the burning rate (*mm/min*), L denotes the burned length (*mm*), and t stands for the burning time (min).

4.4. Shape memory evaluation

The capacity of fabricated bio-composites to return to their original shape under thermal stimulation was evaluated using CP/HP protocols, as displayed in Fig. 7(I). Similarly, recent studies on programmable 4D printed multi-shape gradient metamaterials have demonstrated that multi-material gradient structures can achieve highly controllable, multi-stage shape transformations under thermal or other external stimuli [43]. This assessment aimed to investigate the impact of BC and CSF on the SME attributes of PLA matrix 3D-printed specimens, which measured 30 *mm* in length, 8 *mm* in width, and 1 *mm* in thickness. The experiments were conducted in triplicate, and average values were reported for each series of tests.

In the HP approach, the samples were initially heated to a temperature equal to or exceeding the Tg temperature (T≥Tg). They were then deformed by applying sufficient force within a mould of 20 *mm* in diameter, as depicted in Fig. 7(II). The maximum bending angle achieved, recorded as θ_{max}, was noted during the shape fixation phase (see Fig. 7(II)). After applying the external force and deforming the samples, they were cooled to ambient lab temperature (23 °C). Once stabilised, the mould and force were removed, and the fixed angle was designated as θ_{fixed}. Subsequently, the samples were gradually reheated to maximise recovery before being cooled again. The final bending angle, θ_i, was carefully documented.

In the CP method, the samples were deformed at ambient lab temperature to achieve θ_{max}. The force was then released to record the fixed angle θ_{fixed}, which resulted from residual inelastic strains in the material. Afterwards, a heating–cooling process similar to the HP method was applied. Finally, θ_i was measured to show the extent of partial or full

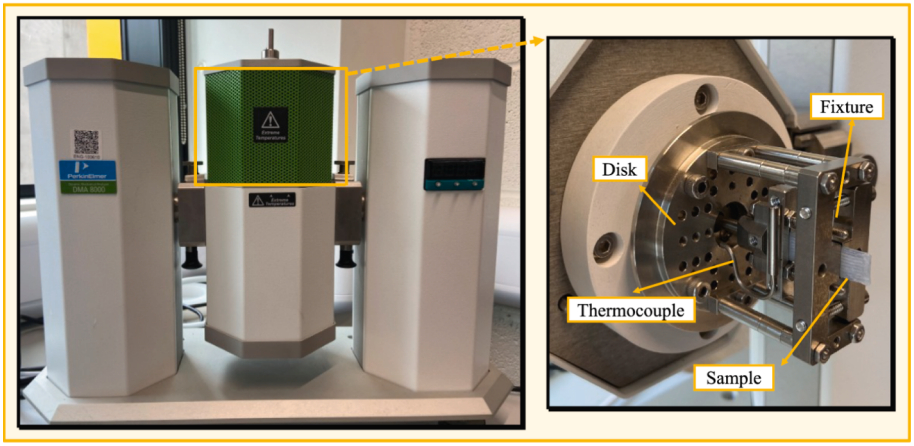

Fig. 6. Schematic presentation of the DMA test setup.

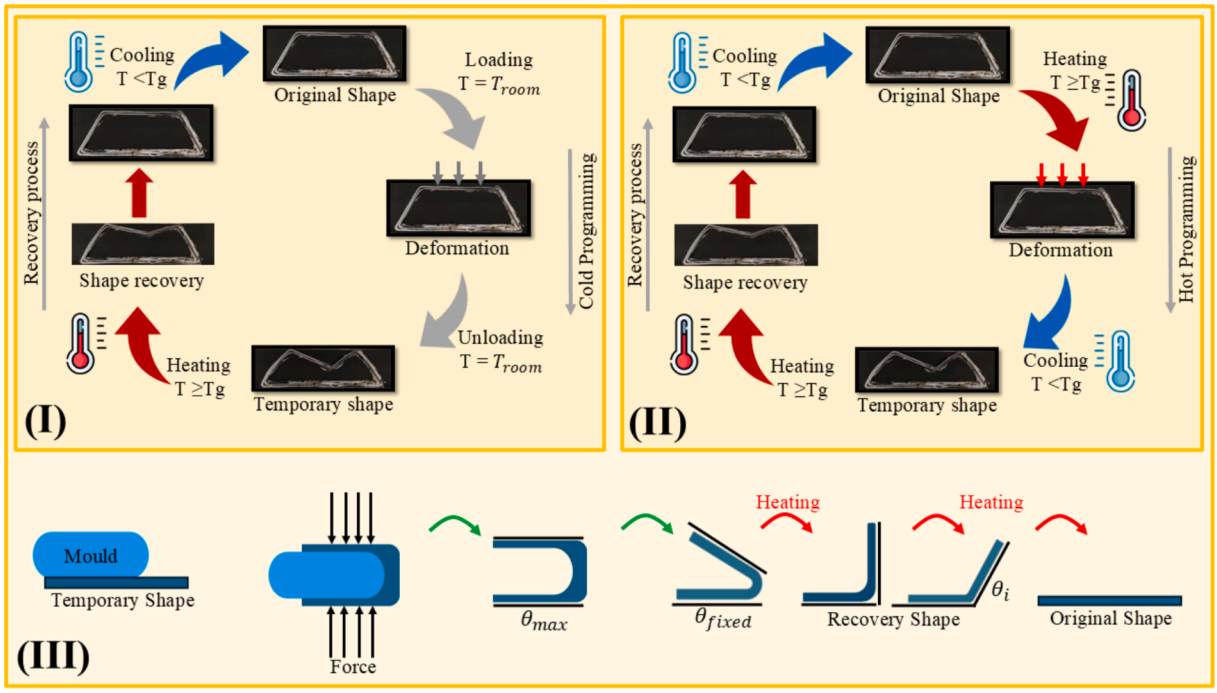

Fig. 7. Schematic explanation of the SME test. (I)-(II) the CP and HP process on the developed bio-composite. (III) bending angle measured at each step.

recovery from the inelastic deformations. Heating of the samples was conducted using a heat gun set to the specified temperature. The samples were positioned vertically and secured at one end. A FLIR E5-XT thermal camera was employed to record and document the sequence of shape recovery. The shape fixation and recovery ratios were calculated based on the angles recorded as follows:

$$\text{Shape fixing (Sf)} = \frac{\theta_{fixed}}{\theta_{max}} \times 100 \tag{4}$$

$$\text{Shape recovery (Sr)} = \frac{\theta_{max} - \theta_i}{\theta_{max}} \times 100 \tag{5}$$

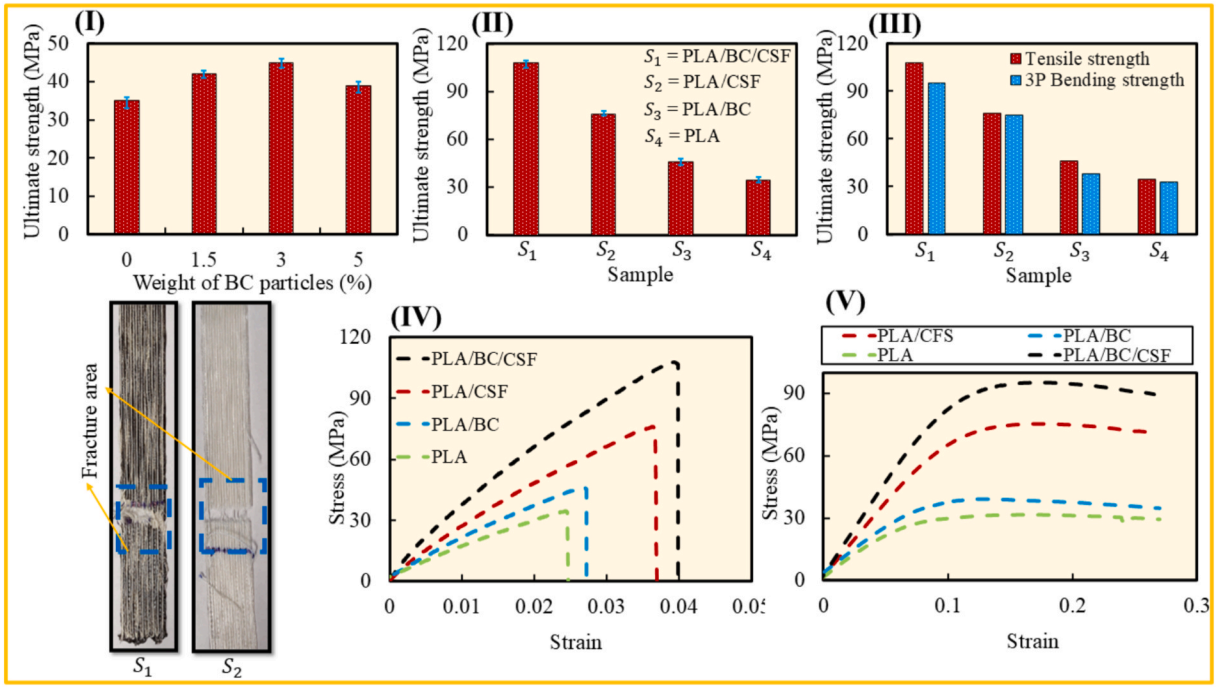

Fig. 8. Mechanical properties of printed bio-composites: PLA, PLA/BC, PLA/CSF, and PLA/BC/CSF. (I) ultimate tensile strength of PLA reinforced with various BC wt.%. (II) ultimate strength of the printed samples. (III) comparison of tensile strength with the three-point bending strength of the printed samples. (IV) and (V) illustrate the stress–strain behaviour of the printed samples under tensile, along with the pictures of broken samples (S_1 and S_2) and three-point bending loading conditions.

5. Results and discussion

This section discusses the mechanical properties of developed bio-composites under quasi static, thermomechanical, and dynamic conditions. Additionally, it covers the flame propagation resistance, shape memory, and microstructural characteristics of the designed bio-composites.

5.1. Mechanical properties

Prior to the CSF reinforcement, the tensile strength of 3D-printed PLA/BC composites with varying BC contents (0%, 1.5%, 3%, and 5 wt%) was evaluated according to the ASTM D638 standard, as illustrated in Fig. 8(I). The results demonstrate a gradual increase in tensile strength with BC content, peaking at 3% by weight, resulting in a 28% enhancement compared to pure PLA. However, higher concentrations of BC led to a reduction in tensile strength, likely due to decreased ductility and the formation of BC clusters within the PLA matrix. This clustering results in micro space separation among the particles, as well as between the particles and the polymer, which hampers effective stress transfer during tensile testing. The mechanical properties of PLA composites containing more than 5 wt% BC were not analysed due to production challenges. Excessive BC content caused inconsistencies in filament production and printing difficulties, preventing the fabrication of high-density samples, which were therefore excluded from further investigation.

Upon identifying the optimal tensile strength in PLA/BC composites, the PLA/BC filament with 3 wt% BC was chosen as the matrix for reinforcement with CSF to further enhance the mechanical properties of the thermoplastics. The tensile and three-point bending characteristics of the CSF-reinforced bio-composite were subsequently assessed in comparison to pure PLA samples, PLA/BC, PLA/CSF, and PLA/BC/CSF.

Fig. 8(II) displays the tensile behaviour of the printed bio-composites: PLA, PLA/BC, PLA/CSF, and PLA/BC/CSF. The inclusion of natural fibres leads to a notable increase in strength, which can be attributed to efficient load transfer at the fibre/matrix interface. The reinforcing effect observed in the present PLA/BC/CSF composites aligns well with previous investigations on additively manufactured continuous fibre-reinforced polymers. For example, Bodaghi et al. [19] reported a significant enhancement in stiffness and thermo-mechanical stability when using modified nozzles and continuous fibres in FFF-printed PLA composites. However, it is noteworthy to mention that the PLA/BC/CSF and PLA/CSF samples are more prone to cracking due to the softer nature of the CSF. The introduction of silk fibre in the PLA/BC bio-composite results in a tensile strength increase of up to 108 MPa, while incorporating silk into PLA can enhance the tensile strength to 76 MPa. This represents an impressive improvement of 213% and 120%, respectively, compared to pure PLA. In contrast, pure PLA exhibits lower strain and strength than the other three composites.

Furthermore, three-point bending tests were conducted to evaluate the bending strength of the printed samples. Fig. 8(III) illustrates a comparison between the three-point bending and tensile strengths, showing that the tensile strength of the PLA/BC/CSF sample is 10% higher than its bending strength. In contrast, pure PLA, which does not contain either BC or CSF reinforcement, demonstrated the lowest strengths, approximately 34 MPa in both tests. Similar to the tensile tests, PLA and PLA/BC samples exhibited lower bending strength when compared to those reinforced with fibres. Specifically, the three-point bending strength of PLA/BC/CSF is 247%, 200%, and 40% greater than that of PLA, PLA/BC, and PLA/CSF, respectively. This reinforces the conclusion that PLA/BC/CSF showcases superior mechanical properties in bending tests, consistent with the findings of the tensile tests. Additionally, Figs. 8(IV) and 8(V) illustrate the elastic-inelastic stress–strain behaviour of the printed bio-composites under tensile with the pictures of broken samples (S_1 and S_2) and three-point bending loads. It is seen that PLA/BC/CSF, PLA/CSF, and PLA/BC exhibit greater stiffness and can endure more strain in both tension and bending compared to pure PLA, respectively.

5.2. Dynamic mechanical analysis

The storage modulus and Tg are essential thermodynamic parameters that highly influence the SME in bio-composites. Evaluating these parameters is crucial for understanding the shape memory behaviour of 4D-printed samples, particularly concerning the effects of incorporating CSF and bamboo charcoal BC particles into PLA. Figs. 9(I) and 9(II) demonstrate the tan δ and storage modulus values for both pure PLA and the bio-composites, respectively, where a prominent peak in tan δ corresponds to the T_g. The findings indicate that the storage modulus of PLA/BC/CSF and PLA/CSF is 3.6 and 2.3 times greater, respectively, than that of pure PLA. This high storage modulus observed for PLA/BC/CSF composites is attributed to the reinforcement provided by continuous fibres, which limit polymer chain mobility and improve load transfer within the matrix. Furthermore, the tan δ value for the reinforced composites is lower than that of pure PLA, suggesting that the printed composites possess enhanced stiffness and strength. More specifically, the tan δ for pure PLA is reported at 2.58, whereas for PLA/BC/CSF, it measures only 0.66. In Fig. 9(I), the T_g of pure PLA is approximately 62°C, while the T_g values for PLA/BC/CSF, PLA/CSF, and PLA/BC are around 63.3 °C, 63.5 °C, and 64.5 °C, respectively. Similar trends in storage modulus for fibre-reinforced polymer composites have been reported in previous studies [24]. All samples were evaluated at temperatures exceeding their T_g to ensure consistent shape memory performance.

5.3. Microstructure study

The microstructural study was conducted on the surface of the PLA/BC/CSF bio-composite to gain a clearer understanding of the BC particle distribution and CSF within the PLA matrix. Fig. 10(I) presents SEM micrographs, depicting the microstructure of the flat and fracture surfaces of the PLA/BC/CSF tensile specimen. Fig. 10(Ia) reveals strong contact at the fibre–matrix interface, with minimal voids, indicating effective impregnation and wet-out in the samples. During tensile testing, areas of the matrix exhibited fracture and damage due to the applied tensile stress. This damage included fibre breakage, with some fibrils pulled out from the silk fibres (See Fig. 10(Ib, c and d)). In other areas, BC particles were observed at the interface, potentially enabling mechanisms that stop or divert cracks. This phenomenon could explain the increased strength observed when BC is added to PLA and PLA/CSF composites. The robust bonding at the fibre–matrix interface, as seen in Fig. 10(I), is attributed to both chemical interactions and mechanical interlocking between the PLA matrix and the fibres. The silk fibres enhance interfacial adhesion by increasing surface roughness and promoting compatibility with the PLA matrix, leading to effective stress transfer during mechanical loading. The formation and propagation of cracks, as illustrated in the SEM images, are primarily due to the brittle nature of the PLA matrix, which fractures under tensile stress. However, the presence of well-dispersed BC particles at the interface helps to inhibit crack growth and enhance the composite's resistance to failure. The fibre pull-out phenomenon indicates the matrix's partial failure to retain the fibres during fracture. This occurrence typically signifies the relative weakness of the matrix compared to the fibre strength, but also reflects an energy dissipation mechanism that contributes to the composite's toughness.

Accurately determining the fibre volume fraction is essential for developing printed composites, as it serves as a fundamental indicator of composite quality and directly impacts mechanical properties and performance. To assess this, the volume fraction of silk fibres in the PLA bio-composite was measured using ImageJ software. A cross-section of a manufactured PLA/BC/CSF sample was cut, divided into three parts,

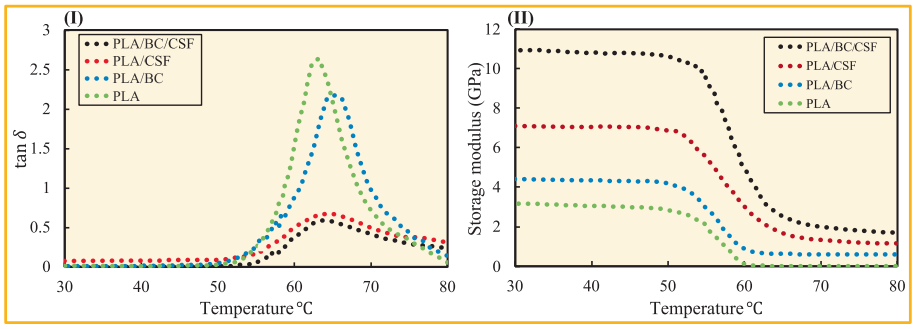

Fig. 9. Variation of (I) storage modulus, and (II) tan δ as a function of temperature for the printed bio-composites.

and SEM images of each section were taken. The acquired images were converted to grayscale, and thresholding was applied to distinguish the silk fibres from the PLA matrix. The fibre area fraction was calculated as the ratio of the segmented fibre area to the total cross-sectional area. Under the assumption of uniform fibre distribution, the measured area fraction was taken as an approximation of the fibre volume fraction. Multiple images from different regions of each cross-section were analysed, and the reported fibre volume fraction 40% represents the average value. The images were then analysed with ImageJ, as shown in Fig. 10(II), to estimate the percentage of silk fibres, or the fibre volume fraction. A similar process was conducted for the PLA/CSF composite sample, yielding comparable results to those of the PLA/BC/CSF sample.

A comparison between the as designed and printed cross-sections of the fibre arrangement is provided to demonstrate the truth of the printing process (Fig. 11(I)). Based on the initial nozzle design and the observed cross-sectional geometry of the extruded filament (Fig. 11(II)), the fibre volume fraction was estimated by assuming a circular fibre cross-section and a rectangular matrix cross-section. Using a fibre diameter of 0.25 *mm* and a matrix cross-section of 0.6 *mm* × 0.2 *mm*, the theoretical fibre volume fraction was calculated to be approximately 40%, which is consistent with the fibre volume fraction obtained from the ImageJ analysis of the printed samples. The reduced matrix cross-sectional dimension compared to the initial nozzle diameter is attributed to a decreased matrix extrusion rate caused by fibre-induced flow blockage and increased pressure drop during extrusion.

5.4. Flame-retardant properties

Flame retardant tests were conducted on the fabricated composite samples, with the results illustrated in Fig. 12. The findings demonstrated that the incorporation of sustainable materials, such as CSF and BC particles, significantly reduced the burning rate by forming protective layers that slow the penetration of heat and volatiles into the composite. Additionally, Figs. 12(I-IV) displays the post-burn appearance of the samples. The CSF-reinforced samples exhibited less complete combustion compared to those without silk fibres. Pure PLA delivered the highest burning rate due to its rapid decomposition during combustion, while the PLA/BC/CSF and PLA/CSF composites displayed superior flame resistance, reducing the burning rate by 41% and 34%, respectively, when compared to pure PLA. The PLA/BC composite improved by 29.5% over pure PLA, as indicated in Fig. 12(V).

The flammability of PLA and its composites was evaluated using UL-94, LOI, and cone CCT. The findings are detailed in Table 2. The LOI results, expressed as the minimum oxygen concentration required to sustain combustion, showed that pure PLA had an LOI of 20.5%. Incorporating BC slightly improved flame resistance, while the combined addition of CSF and BC produced higher LOI values. The PLA/BC/CSF composite achieved the highest LOI of 33.9%, mainly due to the formation of a compact char layer acting as a thermal and physical barrier that limits oxygen diffusion and heat transfer. Moreover, the UL-94 rating of PLA improved from “No Classification” to V-1 with the addition of CSF and BC. This behaviour aligns with findings reported in the reference [44], where the char layer formed during the combustion of natural fibre-reinforced composites has been shown to improve flame retardancy by promoting thermal insulation and reducing combustibility.

The cone calorimeter test results further confirmed these improvements. The peak heat release rate (pHRR) values of PLA/BC/CSF, PLA/CSF, and PLA/BC decreased by 40.3%, 30.4%, and 21%, respectively, compared to pure PLA, indicating improved fire performance. This protective layer directly contributes to the observed reduction in pHRR values [44]. The incorporation of CSF and BC also delayed the time to ignition (TTI) due to the formation of a continuous char network that restricted heat flow. However, BC alone slightly reduced the TTI of PLA because it promotes heat absorption and earlier degradation. In contrast, CSF enhanced structural stability, reduced dripping, and extended the burning time, demonstrating a synergistic improvement in the overall flame retardancy of the composites [19].

5.5. Shape memory property

The shape memory behaviour of PLA-based composites (PLA, PLA/BC, PLA/CSF, and PLA/BC/CSF) was evaluated through cold and hot programming techniques. The samples were tested in a vertical orientation, with temperature monitored using thermocouples and infrared cameras. The objective of this study was to investigate the effect of BC particles and CSF reinforcements on the SME.

Fig. 13 illustrates the original, temporary, and recovered shapes of the PLA/BC/CSF sample under both cooling and hot programming. The results show that PLA/BC/CSF has SME properties, while hot programming, represented in Fig. 13(II), showed enhanced shape fixation for the PLA/BC/CSF composite. The results demonstrate that the residual deformation caused by loading is partially recoverable in the bio-composite after cold/hot programming, marking a notable advancement for this class of materials. Fig. 13(III) underscores the shape fixation performance of bio-composites. In hot programming, the ability to retain shape improved with higher temperatures, with pure PLA exhibiting the best retention. Conversely, in cold programming, the PLA/BC/CSF composite showed reduced shape retention owing to the increased stiffness at ambient lab temperature. The presence of CSF diminishes PLA’s shape recovery owing to its hardness and stiffness, and weak bonding between the fibres and the PLA matrix may lead to separation, further impeding shape recovery [24]. As indicated in Fig. 13 (IV), pure PLA requires 7 s to recover its shape, while PLA/BC, PLA/CSF, and PLA/BC/CSF recover in 6.5, 5.5, and 4.4 s, respectively. This variation is attributed to the relative softness of BC particles compared to CSF. These findings are consistent with the results from the three-point bending test. Fig. 13(V) presents a comparison of shape recovery ratios, revealing that pure PLA achieved the highest recovery, with 97.1% during cold programming and 98.8% during hot programming. PLA/BC also performed satisfactorily, but the PLA/BC/CSF composite exhibited the lowest recovery ratio. The addition of BC particles and CSF

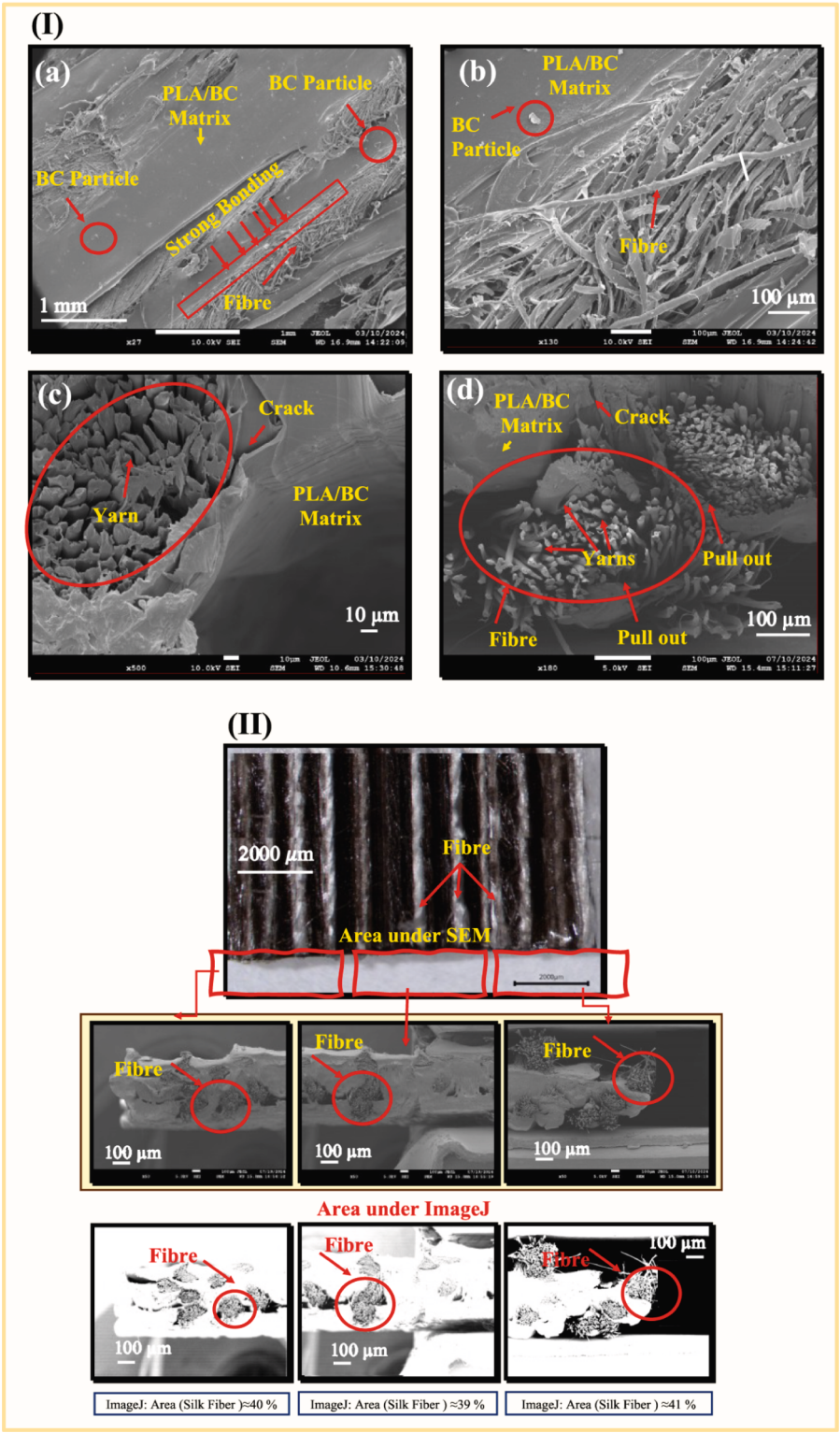

Fig. 10. SEM Results: (I) the microphotograph of the proposed PLA/BC/CSF bio-composite. (II) volume fibre fraction.

diminished the shape recovery capacity of the composites, particularly for those reinforced with fibres.

6. Meta-composite structures

Honeycombs and trapezium-shaped metamaterials were developed using the developed PLA/BC/CSF bio-composite through 3D printing. To assess the mechanical properties of the printed metamaterials, cyclic compression and three-point bending tests were performed. In the compression test, a 50 kN load cell was utilised to compress the samples at a rate of 5 *mm/min*, cyclically reducing their height to 45% of the original (18 *mm*) before complete unloading. Additional tests conducted at 25% compression evaluated the effects of lower loads. Fig. 14(I) and 14(II) show the designed trapezium metamaterial along with its geometric specifications and the printed metamaterials, respectively. The geometric dimensions include a= 73 *mm*, b= 45 *mm*, c= 18 *mm*, l= 12

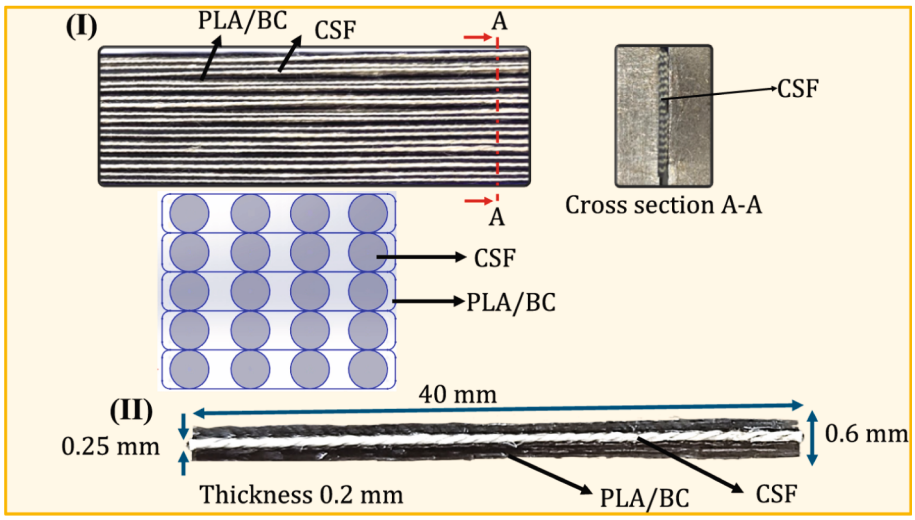

Fig. 11. (I) A comparison between the as-designed and printed cross-sections of the fibre arrangement (II) the one-layer plane view of the geometry of the extruded filament composite PLA/BC reinforced with CSF.

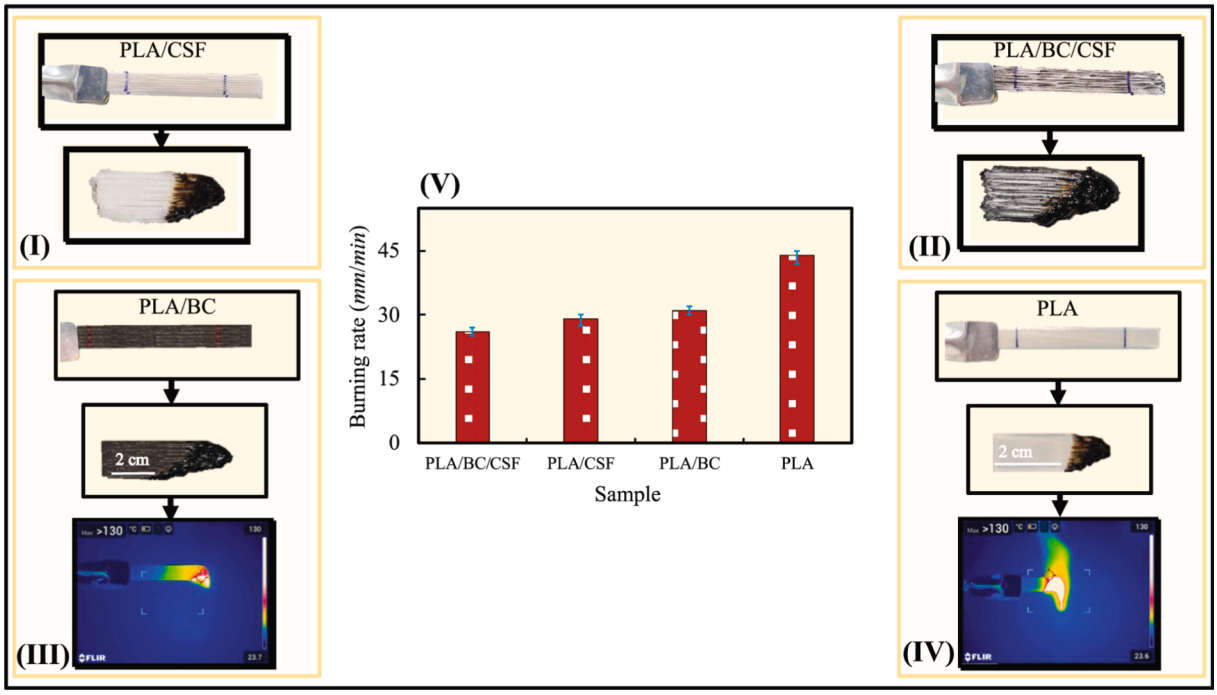

Fig. 12. Burning rate assessment of printed composite samples. (I-IV) post-burn appearance of the samples. (V) burning rate results.

Table 2
UL-94, LOI and CCT results for PLA and PLA composites.

UL-94 (Vertical)					
Samples	Dripping	Rating	LOI(vol.%)	pHHR (kW/m^2)	TTI (s)
PLA	Yes	NC*	20.5	424	56
PLA/BC	Yes	NC	25.3	337	61
PLA/CSF	Yes	V2	30.8	295	63
PLA/BS/CSF	Yes	V1	33.9	253	71

* No Classification (NC).

mm, and $t = 2$ *mm*. As depicted in Fig. 14(III), a trapezium unit cell made from PLA/BC/CSF can support approximately 430N under 45% compression (8.1 *mm* displacement). During loading, the metamaterial exhibits a quasi-constant force of approximately 370N over a plateau region of about 3 *mm*. The input kinetic energy is converted into the elastic and/or inelastic energies and mechanical buckling instability during the quasi-constant force response. The metamaterial absorbs and dissipates the energy (area below force–displacement curve), and consequently, can regulate the force. The quasi-constant force feature is desired for over-load protection as both the structure and external impactor do not experience higher forces and could prevent damage during compression. It is also seen that the trapezium meta-composite structure unloaded exhibits a residual inelastic deformation of 4 *mm* under 45% compression, while no residual strain is observed under 25% compression. Following 45% compression loading, the trapezium structure was heated and subsequently cooled to ambient laboratory temperature under the shape recovery process. The results indicate that the trapezium structure almost returned to its original shape.

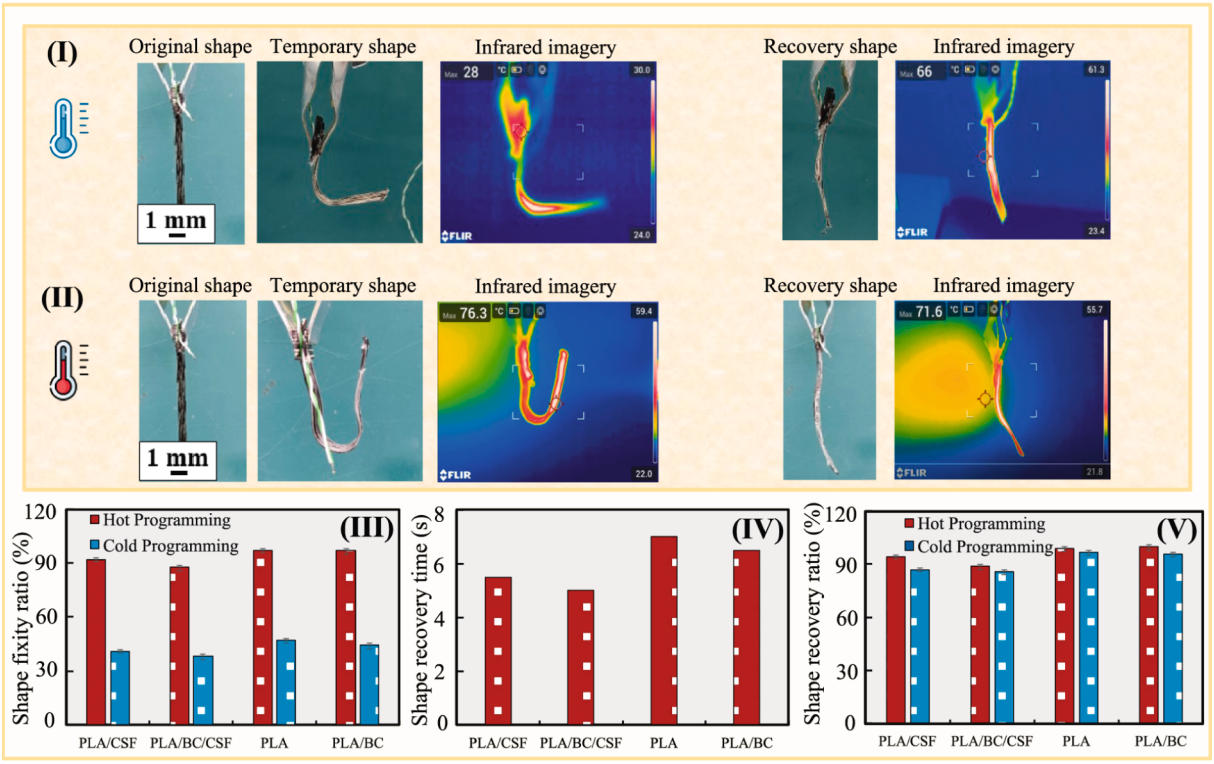

Fig. 13. Shape memory test results. (I) original, temporary, and recovered shapes of cold-programmed printed PLA/BC/CSF. (II) original, temporary, and recovered shapes of hot-programmed printed PLA/BC/CSF, illustrated with infrared images at the initiation of cooling. (III) shape fixity ratio of bio-composites under cold/ hot programming. (IV) shape recovery time of bio-composites under cold/ hot programming. (V) shape recovery ratio of bio-composites under cold/ hot programming.

Furthermore, Fig. 14(IV) illustrates the three-point bending response of the cellular structure. It is seen that the structure can sustain 33 N up to 3.5 *mm* displacement, after which the bending force begins to decrease showing a negative stiffness. Mode shapes of the unit cell under both compression and bending tests were also analysed to confirm the reliability of the mechanical tests. Figs. 15(I) and 15(II) display the mode shapes of the trapezium unit cell under 45% compression and during three-point bending, respectively. Fig. 15(I) displays that the trapezium meta-composite buckles into a saddle shape on the top side at the start of the plateau region (u=3.24 *mm*). This returnable buckling mode persists until 4.5 *mm*, after which the structure exhibits plastic hinge behaviour due to elastic-inelastic material properties. In Fig. 15(II), the *meta*-structure maintains a returnable bending mode under the three-point bending test up to u=5 *mm*, after which a permanent buckled shape with rigid struts forms.

Additionally, Figs. 16(I) and 16(II) present the CAD designs and printed honeycomb metamaterials, respectively. The dimensions are d= 35 *mm*, k= 2 *mm*, and L= 12 *mm*. Fig. 16(III) demonstrates the force–displacement behaviours of the printed honeycomb metamaterial made of PLA/BC/CSF. It is seen that the metamaterial, composed of three honeycomb unit cells, can endure up to 400N under 36 *mm* of compressive displacement. By unloading after 60% compression and allowing the structure to rest for 2 h, the metamaterial exhibits a residual inelastic displacement of 19 *mm*. However, no residual displacement is seen under maximum 30% compression. The structure under 30% and 60% compression levels shows non-linear elastic and elastic-inelastic behaviours and dissipates energies (hysteresis loops). Moreover, to evaluate the shape memory of the printed honeycomb and its mechanical integrity, the structure was subjected to two cycles of 60% compression. Following the first loading–unloading cycle, the structure was heated above its Tg and then cooled to the ambient lab temperature. The shape recovery ratio, which compares the restored height to the initial height, indicates an 85% recovery post-heating–cooling, underscoring its reusability. The force–displacement results show that the second cycle experienced a 20% reduction in force level due to the residual strain from the first cycle. It reveals that the meta-composite structure undergoing large deformations can be used repeatedly. According to the energy absorption characteristics, the mechanical results indicate that the honeycomb structure dissipates 5.38 J during the first hysteresis cycle. During the second cycle, the dissipated energy is reduced to 3.21 J, a decrease of approximately 40%, which can be attributed to residual strain remaining after shape recovery process.

The lightweight and high energy absorption characteristics of cellular structures like sandwich structures have resulted in their popular adoption in engineering sectors. By increasing the quantity of cellular units in the lightweight design and optimising the strength-to-weight ratio, the overall strength can be tuned for various applications. By considering the shape-memory energy-absorbing bio-composites developed in this study, cellular structures could hold promise for usage in construction, logistics, automotive, and aerospace industries, paving the way for more sustainable, safe, and efficient solutions across diverse sectors.

7. Application

The proposed PLA/BC/CSF bio-composite delivers substantial gains in mechanical performance, flame resistance, and shape recovery while advancing sustainability. Critically, the FGF pellet-fed extrusion printing used here eliminates the filament-making step, which otherwise adds processing time, energy consumption, and avoidable scrap. By directly extruding pellets, the process is cheaper, faster, and more suitable when time, energy, and material budgets are constrained. The integrated continuous-fibre deposition enables in-situ reinforcement during printing, improving stiffness/strength and supporting elastic recoverability and energy absorption in architected parts. This section is focused on potential applications of honeycomb and trapezium meta-

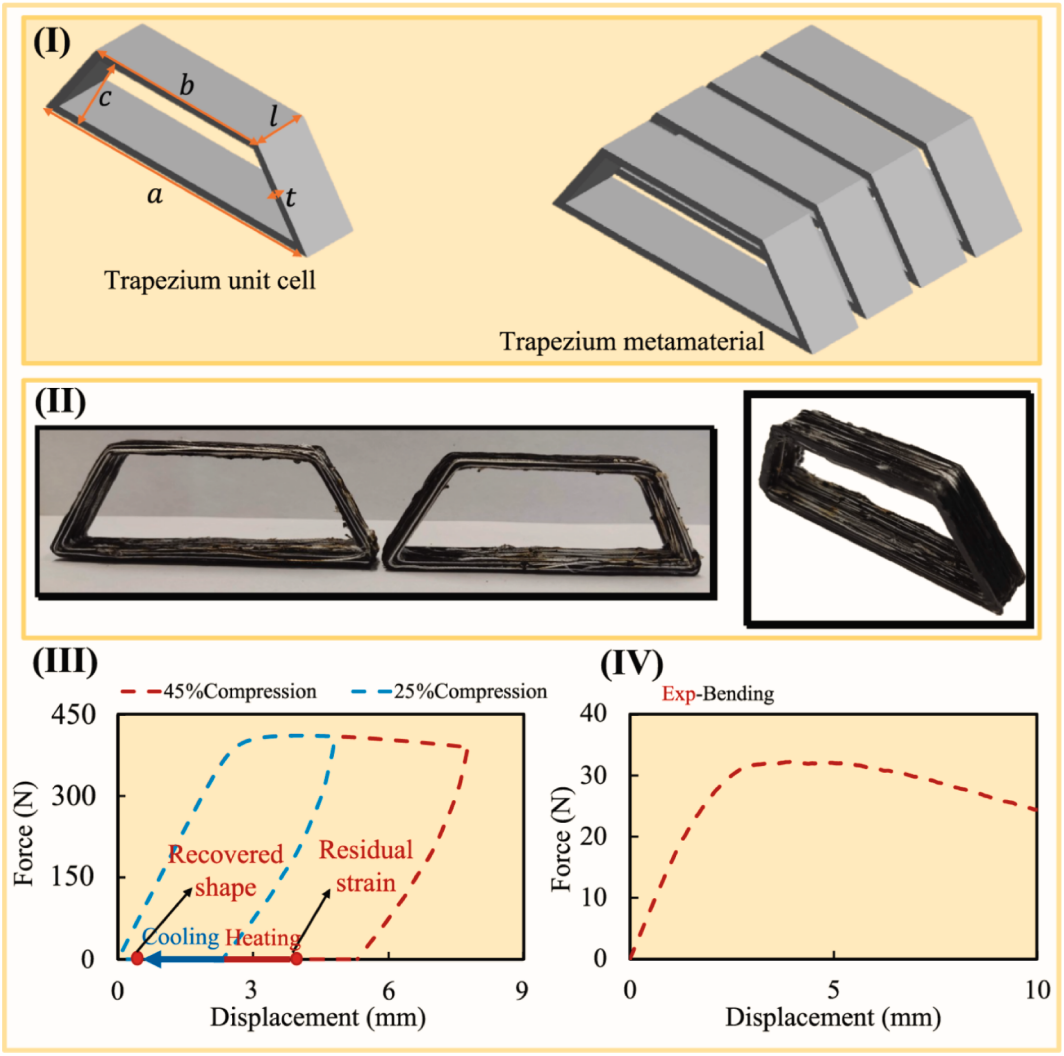

Fig. 14. Mechanical properties of the trapezium unit cell fabricated from PLA/BC/CSF bio-composite. (I) Schematic layout of the designed unit cell. (II) 3D-printed unit cells. (III) force–displacement response under cyclic compression loading at 45% and 25% levels. (IV) force–displacement behaviours under the three-point bending test.

composite structures printed for logistics and automotive applications.

Sandwich structures using PLA/BC/CSF honeycomb or trapezium unit-cell cores could deliver high bending stiffness-to-weight with tuneable energy dissipation and damage tolerance. The cellular cores dissipate impact energy and limit face-sheet denting, while the bio-composite's heat-activated shape recovery enables rapid, low-cost repair after overloads. For micro-mobility, trapezium-cored panels can be integrated into an e-scooter chassis (Fig. 17) as deck, spine, or battery-guard members, reducing mass and improving ride comfort via quasi-zero stiffness and passive energy dissipation. Together, these features offer a simple, sustainable alternative to metal ribs and active energy absorbers without sacrificing structural performance.

Perforated-body pallets with trapezium-shaped legs would deliver lighter weight, easier wash-down, and efficient nesting/stacking for warehouses and shipping, see Fig. 17. The open grid cuts material usage without sacrificing strength, while trapezium stands boost bending stiffness, energy dissipation, and provide clear forklift/pallet-jack entry for smooth handling under heavy loads. Under drops/impacts, the cellular geometry exhibits a quasi-zero-stiffness response and a force plateau that dissipates energy and caps transmitted impacts, reducing damage to fragile loads. If impacts cause local buckling and inelastic deformations, the PLA/BC/CSF's heat-triggered shape recovery enables fast on-site repair, extending service life, reducing waste, and improving total cost and sustainability.

The study evaluates PLA/BC/CSF pallets against the 10R circular-economy framework [45]. As shown in Fig. 17, the design supports multiple R-strategies across use and end-of-life: reduced material via the perforated body (R2), reusability (R3), on-site repair through heat-activated shape recovery (R4), refurbish/remanufacture after damage (R5-R6), repurposing of modules (R7), and mechanical recycling or, if needed, recovery (R8-R9). The shape-memory effect is pivotal, enabling rapid recoverability after deformation, extending service life, and cutting waste, cost, and downtime. Collectively, these features position the pallets as a practical, circular solution.

To assess service-temperature performance, printed PLA/BC/CSF was benchmarked against neat PLA at conditions relevant to vehicle interiors, for instance, where car dashboard surfaces can approach ~70 °C in summer. Rectangular beams of each material were conditioned in a laboratory oven at 70 °C for 1h (Fig. 18I). Ventilation was set to 20%, and a 60 g mass was placed at mid-span to apply a constant bending load throughout exposure. Post-test inspection (Fig. 18II) showed pronounced thermal creep and progressive sagging in PLA under the combined thermal–mechanical load. In contrast, PLA/BC/CSF maintained its geometry with no visible deformation, confirming superior thermal stability and load-bearing capacity at elevated temperature. These results, together with the composite's demonstrated mechanical

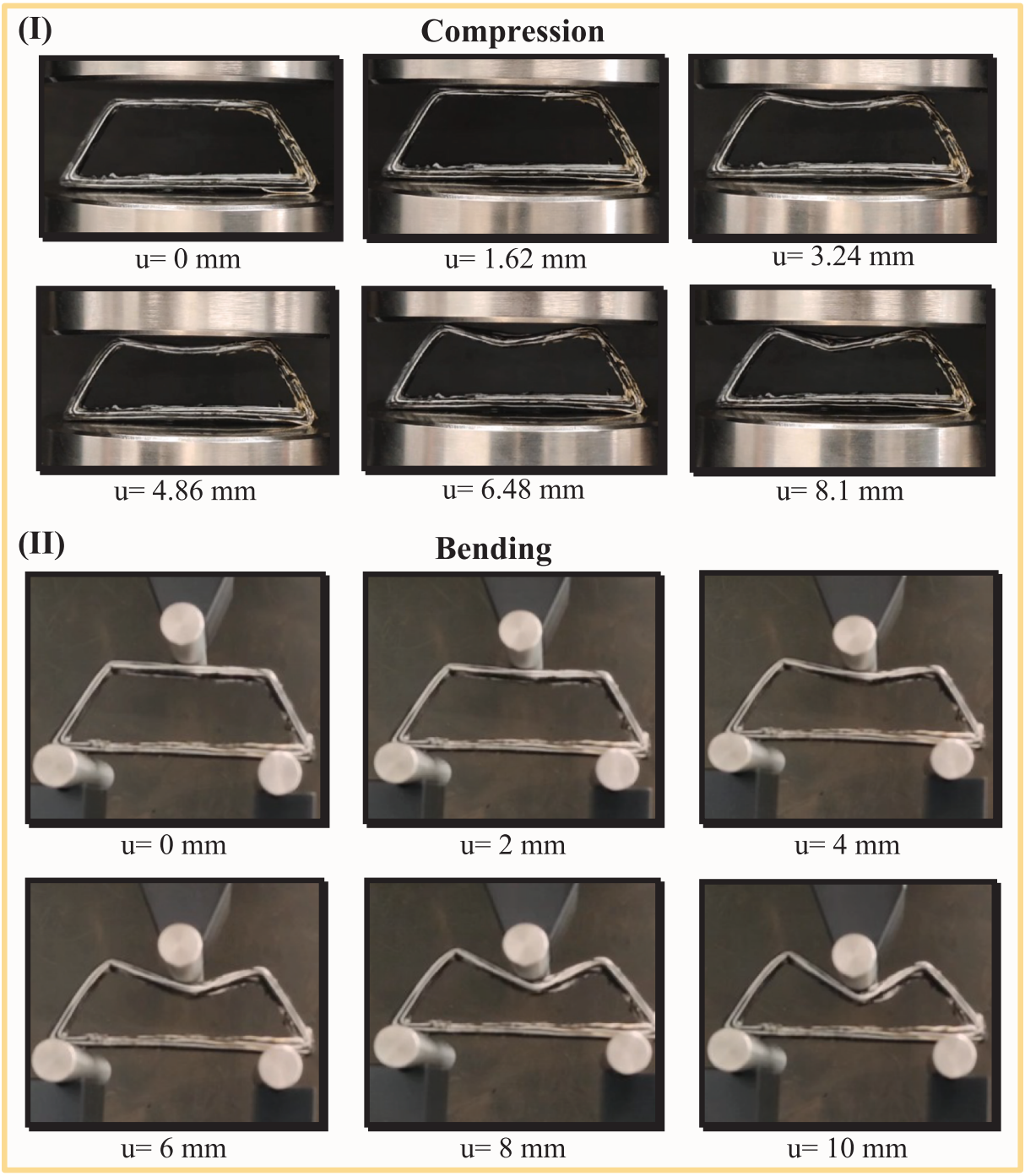

Fig. 15. Mode shapes of the trapezium meta-composite structure. (I) mode shapes under 45% compression. (II) mode shapes under three-point bending.

strength, flame resistance, and heat-activated shape recovery, indicate strong suitability for interior automotive components. A conceptual dashboard manufactured from PLA/BC/CSF (Fig. 18III) illustrates potential integration paths, e.g., instrument-panel substrates, ducts, or local reinforcement ribs. Beyond improved robustness and flame performance, the material's resistance to thermal distortion would help preserve fit and finish over life, while the shape-memory effect enables local heat-assisted recovery after incidental dents or overloads, reducing scrap and maintenance costs. Overall, PLA/BC/CSF offers a lightweight, durable, and sustainable alternative to neat PLA or conventional polymers for warm-zone interior structures.

8. Conclusion

A pellet-fed material-extrusion platform with integrated continuous-fibre co-deposition was developed to produce PLA/BC/CSF biocomposite that addresses the strength, flammability, and thermal-creep limitations of neat PLA. The system enables direct printing from pellets, broadening material choice while reducing time, energy, and waste relative to filament routes. Mechanical, thermo-mechanical, flammability, shape-memory, and architected-structure evaluations demonstrate that high, recoverable performance can be achieved with bio-based constituents. Key material/structural/conceptual design findings include:

Tensile strength:

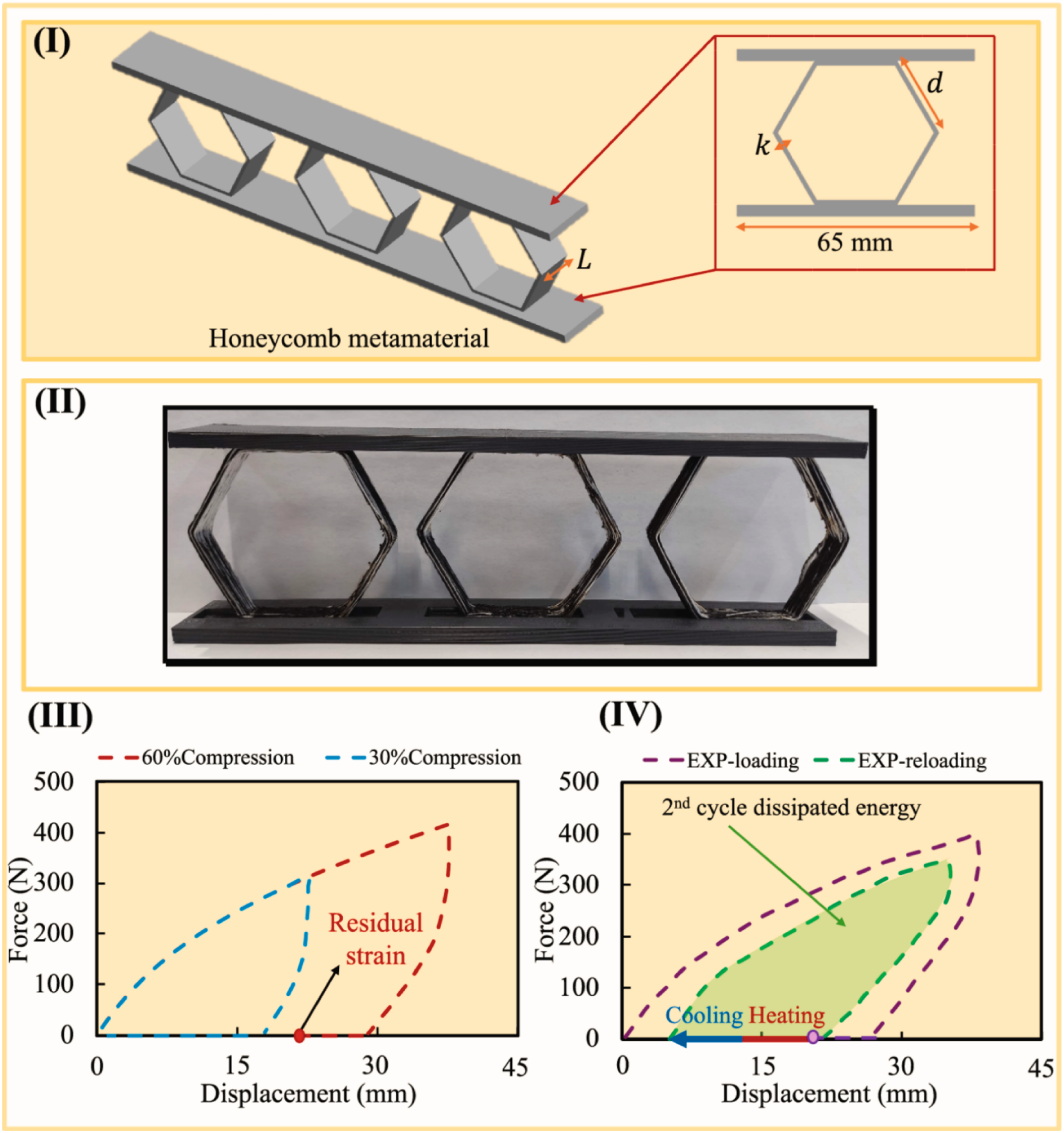

Fig. 16. Mechanical properties of the honeycomb metamaterial fabricated from PLA/BC/CSF bio-composite. (I) schematic layout of the designed metamaterial. (II) 3D-printed honeycomb structure. (III) force–displacement response under cyclic compression at 60% and 30% levels. (IV) force–displacement and energy dissipation characteristics over multiple cycles following the shape recovery process.

- PLA/BC (3 wt% BC): +28% tensile strength improvement vs PLA (optimal BC).
- PLA/CSF: 76 MPa tensile strength with +120% improvement vs PLA.
- PLA/BC/CSF: 108 MPa tensile strength with +213% improvement vs PLA.

Bending strength:

- PLA/BC/CSF: +247% (vs PLA); +200% (vs PLA/BC); +40% (vs PLA/CSF).

Flammability:

- UL-94 horizontal burning-rate reductions 41% (PLA/BC/CSF), 34% (PLA/CSF), 29.5% (PLA/BC) vs PLA and UL-94 vertical, attaining a V-1 rating and an LOI of 33.9 vol%, evidencing marked flame-retardant improvements with BC and CSF additives.

Shape recovery:

- PLA has highest recovery.
- PLA/BC/CSF has fastest recovery time (~ 4.4 s).
- Honeycomb structure shows ~85% inelastic deformation recovery after 60% compression with heat. It has a full elastic recovery at 30%.

Thermal-mechanical stability:

- Under load test (70 °C, 60 g, 1h): PLA exhibits creep/sagging; PLA/BC/CSF retained geometry.

Meta-composite structures and performance:

- Trapezium unit cell: Sustained ~33 N up to 3.5 *mm* in bending mode followed by a force drop (negative-stiffness region). Support ~ 430*N* under 45% compression showing energy-dissipation and quasi-constant force and quasi-zero stiffness.
- Honeycomb unit cell: Withstood ~400 N at 36 *mm* compression; energy-dissipation loops; reuse enabled by heat-activated shape recovery.

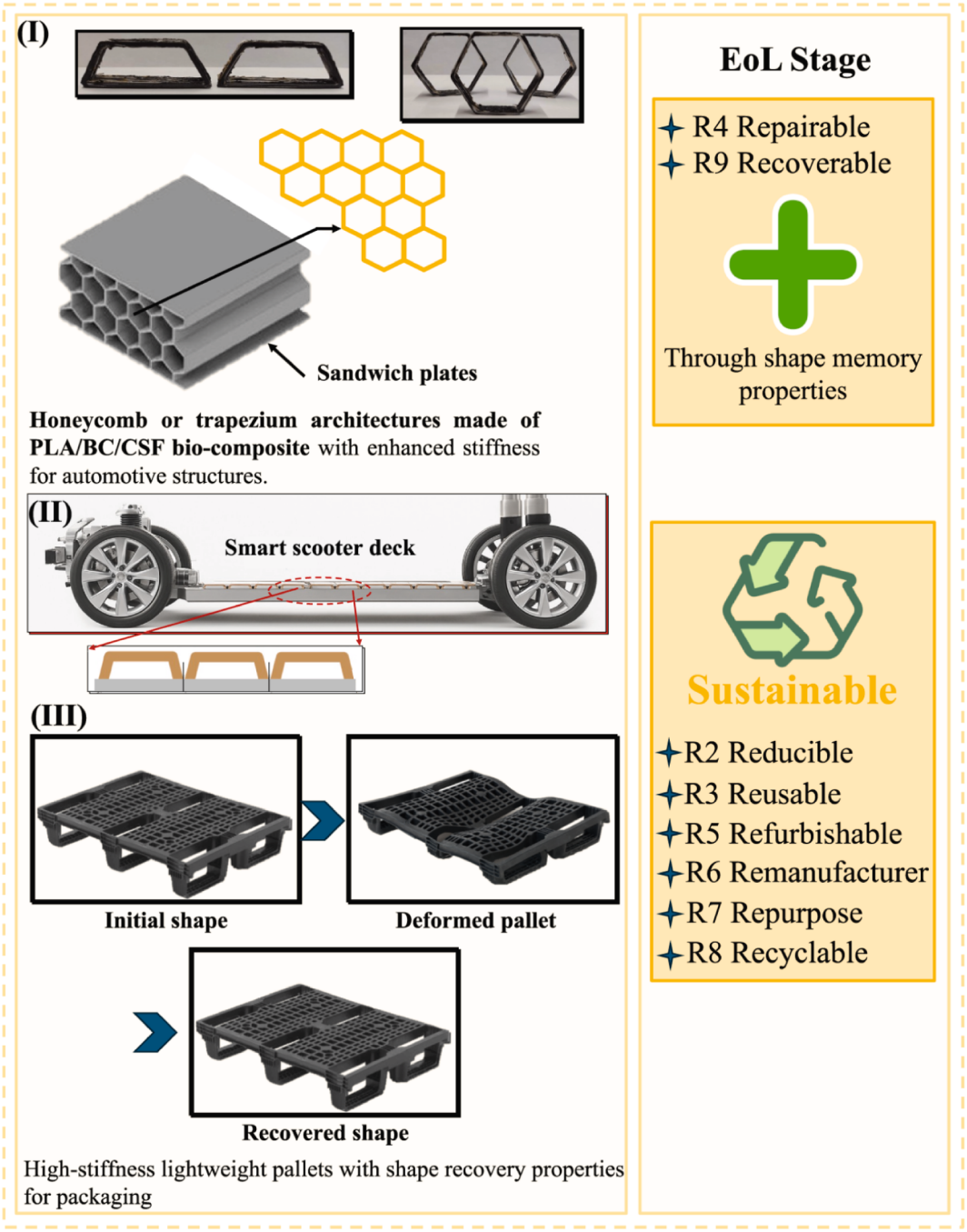

Fig. 17. Applications of PLA/BC/CSF architected bio-composites. (I) honeycomb and trapezium unit cells used as sandwich-panel cores. (II) integration as lightweight members in a micro-mobility chassis. (III) perforated pallets showing initial, damaged, and heat-recovered states. Right panels map alignment with 10R strategies (R2-R9), emphasising repairability and recoverability via shape-memory effects. Overall benefits include low mass, high stiffness, energy dissipation with quasi-zero-stiffness behaviour, and rapid on-site repair, supporting circular, durable products.

Conceptual design applications:

- Perforated logistics pallets: Lower mass, easy wash-down, clear fork entry; quasi-zero stiffness response and dissipation limit impact to fragile loads; local heat-recovery extends life; alignment with 10R strategies.
- Automotive interior: Dashboard face-sheet/trim printed in PLA/BC/CSF resists ~70 °C distortion and is recoverable after dents; chassis inserts/sandwich cores offer lightweight stiffness and passive energy dissipation.

A scalable, filament-free route to high-performance bio-composites is thereby established, enabling circular logistics and micro-mobility applications. Further optimisation of fibre architecture, durability, and recyclability is anticipated toward production deployment.

CRediT authorship contribution statement

Kaveh Rahmani: Writing – review & editing, Visualization, Validation, Methodology, Investigation, Formal analysis, Data curation, Conceptualization. **Shawn Ravanbod:** Writing – original draft, Visualization, Investigation. **Mohammadreza L. Dezaki:** Writing – review &

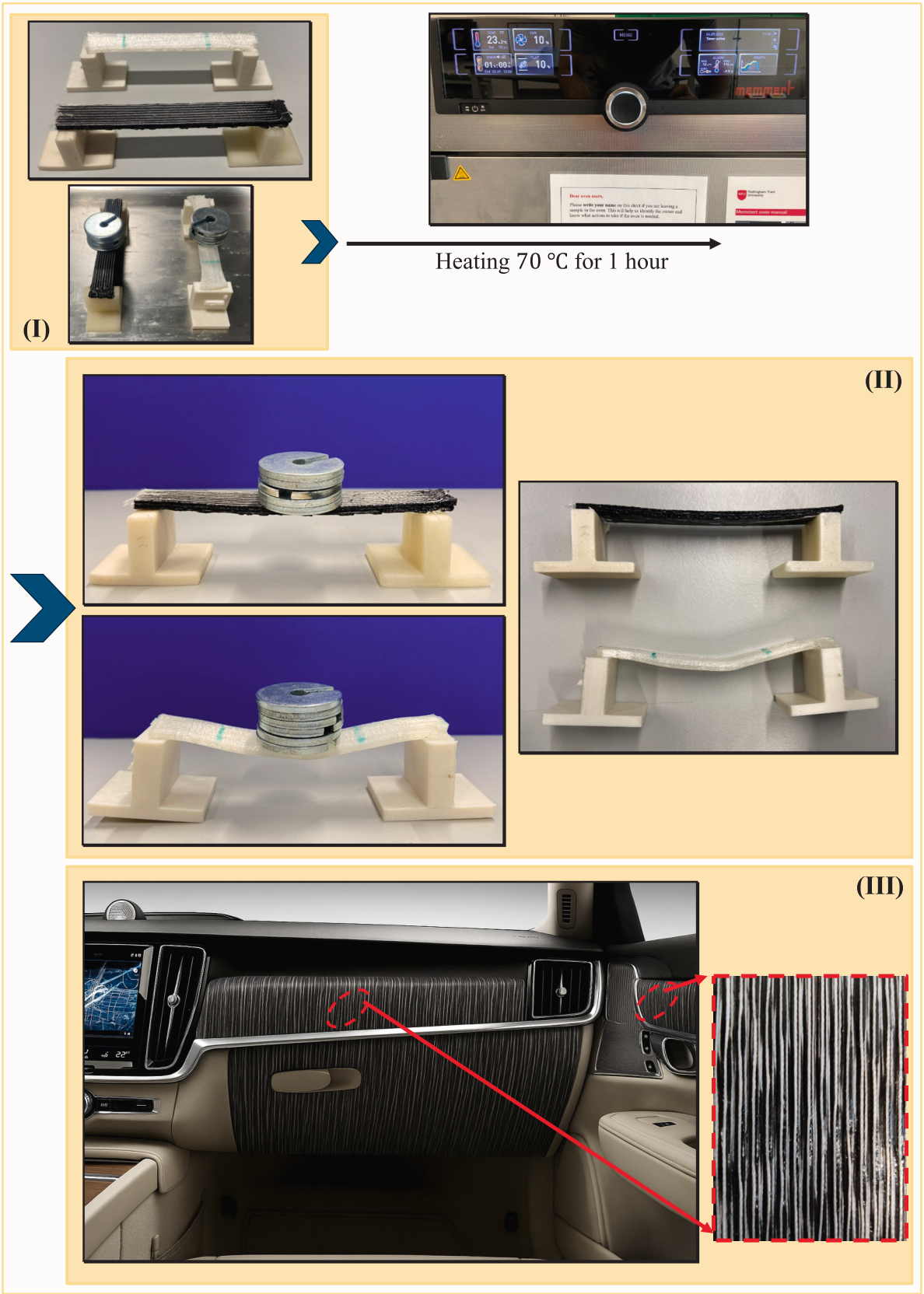

Fig. 18. Thermal-mechanical comparison of PLA/BC/CSF vs neat PLA at 70 °C. (I) printed specimens and loading/oven setup. (II) post-test outcome: pronounced creep/sagging in PLA, negligible change in PLA/BC/CSF. (III) a conceptual dashboard prototype using the bio-composite.

editing, Methodology. **Callum Branfoot:** Writing – review & editing, Methodology, Investigation. **Mahdi Bodaghi:** Writing – review & editing, Writing – original draft, Visualization, Supervision, Resources, Project administration, Methodology, Investigation, Funding acquisition, Conceptualization.

Declaration of competing interest

The authors declare that they have no known competing financial interests or personal relationships that could have appeared to influence the work reported in this paper.

Acknowledgements

This work was supported by the Engineering and Physical Sciences Research Council (EPSRC) [award number: EP/Y011457/1, project: I5M]; and the EPSRC's Innovation Launchpad Network+ Researcher in Residence scheme [grant numbers: EP/W037009/1, EP/X528493/1; award number: RIR26C230615-6, project: BIO-CYCLE, researcher: Mahdi Bodaghi].

Data availability

Data will be made available on request.

References

[1] G. Struzziero, M. Barbezat, A.A. Skordos, Consolidation of continuous fibre reinforced composites in additive processes: a review, Addit. Manuf. 48 (2021) 102458, https://doi.org/10.1016/j.addma.2021.102458.
[2] W. Ye, H. Dou, J. Liu, Z. Li, Y. Cheng, D. Zhang, F. Yang, S. Jing, Additive manufacture of programmable multi-matrix continuous carbon fiber reinforced gradient composites, Addit. Manuf. 89 (2024) 104255, https://doi.org/10.1016/j.addma.2024.104255.
[3] K. Dong, H. Ke, M. Panahi-Sarmad, T. Yang, X. Huang, X. Xiao, Mechanical properties and shape memory effect of 4D printed cellular structure composite with a novel continuous fiber-reinforced printing path, Mater. Des. 198 (2021) 109303, https://doi.org/10.1016/j.matdes.2020.109303.
[4] R. Wagmare, R. Harshe, J. Pednekar, T.U. Patro, Additive manufacturing of continuous fiber-reinforced polymer composites: current trend and future directions, Prog. Addit. Manuf. 10 (4) (2025) 1973–2000, https://doi.org/10.1007/s40964-024-00777-9.
[5] M. Lalegani Dezaki, M. Bodaghi, 4D printing and programming of continuous fibre-reinforced shape memory polymer composites, Eur. Polym. J. 210 (2024) 112988, https://doi.org/10.1016/j.eurpolymj.2024.112988.
[6] Z. Ding, O. Weeger, H.J. Qi, M.L. Dunn, 4D rods: 3D structures via programmable 1D composite rods, Mater. Des. 137 (2018) 256–265, https://doi.org/10.1016/j.matdes.2017.10.004.
[7] A. le Duigou, D. Correa, M. Ueda, R. Matsuzaki, M. Castro, A review of 3D and 4D printing of natural fibre biocomposites, Mater. Des. 194 (2020) 108911, https://doi.org/10.1016/j.matdes.2020.108911.
[8] C. Yang, X. Xin, W. Zhao, C. Lin, L. Liu, Y. Liu, J. Leng, Highly programmable 4D printed multi-shape gradient metamaterials and multifunctional devices, Int. J. Extreme Manuf. 7 (5) (2025) 055504, https://doi.org/10.1088/2631-7990/add8ca.
[9] P. Cheng, K. Wang, X. Chen, A. Le Duigou, Y. Peng, W. Wen, Compressive property and shape memory effect of 3D printed continuous ramie fiber reinforced biocomposite corrugated structures, Smart Mater. Struct. 31 (12) (2022) 124003.
[10] B. Alcayde, M. Merzkirch, A. Cornejo, S. Jiménez, E. Marklund, L.G. Barbu, Fatigue behaviour of glass-fibre-reinforced polymers: Numerical and experimental characterisation, Compos. Struct. 337 (2024) 118057, https://doi.org/10.1016/j.compstruct.2024.118057.
[11] B. Karaş, P.J. Smith, J.P.A. Fairclough, K. Mumtaz, Additive manufacturing of high density carbon fibre reinforced polymer composites, Addit. Manuf. 58 (2022) 103044, https://doi.org/10.1016/j.addma.2022.103044.
[12] X. Wang, M. Jiang, Z. Zhou, J. Gou, D. Hui, 3D printing of polymer matrix composites: a review and prospective, Compos. B Eng. 110 (2017) 442–458, https://doi.org/10.1016/j.compositesb.2016.11.034.
[13] N. van de Werken, H. Tekinalp, P. Khanbolouki, S. Ozcan, A. Williams, M. Tehrani, Additively manufactured carbon fiber-reinforced composites: State of the art and perspective, Addit. Manuf. 31 (2020) 100962, https://doi.org/10.1016/j.addma.2019.100962.
[14] T.D. Ngo, A. Kashani, G. Imbalzano, K.T.Q. Nguyen, D. Hui, Additive manufacturing (3D printing): a review of materials, methods, applications and challenges, Compos. B Eng. 143 (2018) 172–196, https://doi.org/10.1016/j.compositesb.2018.02.012.
[15] M. Lalegani Dezaki, C. Branfoot, J. Baxendale, M. Bodaghi, Bio-based gradient composites for 3D/4D printing with enhanced mechanical, shape memory, and flame-retardant properties, Macromol. Mater. Eng. 310 (6) (2025), https://doi.org/10.1002/mame.202400276.
[16] K.O. Odesanya, R. Ahmad, M. Jawaid, S. Bingol, G.O. Adebayo, Y.H. Wong, Natural fibre-reinforced composite for ballistic applications: a review, J. Polym. Environ. 29 (12) (2021) 3795–3812, https://doi.org/10.1007/s10924-021-02169-4.
[17] S. Palaniyappan, N.K. Sivakumar, G. Annamalai, M. Bodaghi, P. Saravanamuthukumar, O. Alageel, S. Basavarajappa, M.I. Hashem, Mechanical and tribological behaviour of three-dimensional printed almond shell particles reinforced polylactic acid bio-composites, Proc. Instit. Mech. Eng., Part L: J. Mater.: Des. Appl. 239 (1) (2025) 111–126, https://doi.org/10.1177/14644207241248505.
[18] L. Pezzana, R. Wolff, J. Stampfl, R. Liska, M. Sangermano, High temperature vat photopolymerization 3D printing of fully bio-based composites: green vegetable oil epoxy matrix & bio-derived filler powder, Addit. Manuf. 79 (2024) 103929, https://doi.org/10.1016/j.addma.2023.103929.
[19] M. Bodaghi, K. Rahmani, M.L. Dezaki, C. Branfoot, J. Baxendale, 3D/4D printed bio-composites reinforced by bamboo charcoal and continuous flax fibres for superior mechanical strength, flame retardancy and recoverability, Polym. Test. 143 (2025) 108709, https://doi.org/10.1016/j.polymertesting.2025.108709.
[20] A. Khan, S.M. Sapuan, E.S. Zainudin, M.Y.M. Zuhri, Physical, mechanical and thermal properties of novel bamboo/kenaf fiber-reinforced polylactic acid (PLA) hybrid composites, Compos. Commun. 51 (2024) 102103, https://doi.org/10.1016/j.coco.2024.102103.
[21] M. Bodaghi, L. Wang, F. Zhang, Y. Liu, J. Leng, R. Xing, M.D. Dickey, S. Vanaei, M. Elahinia, S. van Hoa, D. Zhang, K. Winands, T. Gries, S. Zaman, H. Soleimanzadeh, T. Barši Palmić, J. Slavič, Y. Tadesse, Q. Ji, A. Zolfagharian, 4D printing roadmap, Smart Mater. Struct. 33 (11) (2024) 113501, https://doi.org/10.1088/1361-665X/ad5c22.
[22] C. Lin, M. Yang, F. Zhang, Y. Liu, J. Leng, Stimuli-responsive smart materials for biomedical applications, Mater. Sci. Eng.: R: Rep. 167 (2026) 101126, https://doi.org/10.1016/j.mser.2025.101126.
[23] Q. Li, D. Zhang, S. Zhang, J. Soete, S. Lomov, L. Gorbatikh, C. Zeng, Bamboo-inspired 3D printed continuous fiber-reinforced vascular composites, Compos. Commun. 53 (2025) 102219, https://doi.org/10.1016/j.coco.2024.102219.
[24] K. Rahmani, C. Branfoot, S. Karmel, K. Lindsey, M. Bodaghi, Flexible bio-composites with continuous natural fibre and bamboo charcoal: enhanced flame retardancy, mechanical resilience, energy-absorbing & printability performance, Virtual Phys. Prototyping 20 (1) (2025), https://doi.org/10.1080/17452759.2025.2534845.
[25] S. Ravanbod, K. Rahmani, C. Branfoot, S. Karmel, A. Haque, M. Lidgett, A. M. Shahidi, A. Alderson, M. Bodaghi, Biomimetic composite meta-stabilisers with programmable multi-directional quasi-zero stiffness and vibration isolation, Mater. Today Adv. 28 (2025) 100661, https://doi.org/10.1016/j.mtadv.2025.100661.
[26] S. Ravanbod, K. Rahmani, S. Karmel, I. Pande, H. Amel, C. Branfoot, A.M. Shahidi, A. Alderson, M. Bodaghi, From coral to control: bio-inspired, 3D-printable metamaterials with tuneable quasi-zero stiffness and multi-functional bio-composites, Mater. Des. 257 (2025) 114398, https://doi.org/10.1016/j.matdes.2025.114398.
[27] W. Tian, K. Yang, S. Wu, J. Yang, H. Luo, J. Guan, R.O. Ritchie, Impact of hydration on the mechanical properties and damage mechanisms of natural silk fibre reinforced composites, Compos. A Appl. Sci. Manuf. 147 (2021) 106458, https://doi.org/10.1016/j.compositesa.2021.106458.
[28] S. Gupta, H. Alrabaiah, M. Christophe, M. Rahimi-Gorji, S. Nadeem, A. Bit, Evaluation of silk-based bioink during pre and post 3D bioprinting: a review, J. Biomed. Mater. Res. B Appl. Biomater. 109 (2) (2021) 279–293, https://doi.org/10.1002/jbm.b.34699.
[29] P. Gupta, M. Adhikary, M. Kumar, N. Bhardwaj, B.B. Mandal, Biomimetic, osteoconductive non-mulberry silk fiber reinforced tricomposite scaffolds for bone tissue engineering, ACS Appl. Mater. Interfaces 8 (45) (2016) 30797–30810, https://doi.org/10.1021/acsami.6b11366.
[30] A.W. van Vuure, J. Vanderbeke, Y. Mosleh, I. Verpoest, N. El-Asmar, Ductile woven silk fibre thermoplastic composites with quasi-isotropic strength, Compos. A Appl. Sci. Manuf. 147 (2021) 106442, https://doi.org/10.1016/j.compositesa.2021.106442.
[31] C. Vyas, J. Zhang, Ø. Øvrebø, B. Huang, I. Roberts, M. Setty, B. Allardyce, H. Haugen, R. Rajkhowa, P. Bartolo, 3D printing of silk microparticle reinforced polycaprolactone scaffolds for tissue engineering applications, Mater. Sci. Eng. C 118 (2021) 111433, https://doi.org/10.1016/j.msec.2020.111433.
[32] I. Vroman, L. Tighzert, Biodegradable polymers, Materials 2 (2) (2009) 307–344, https://doi.org/10.3390/ma2020307.
[33] Y. Liang, H. Chen, T. Lin, Z. Deng, W. Li, W. Lu, Q. Zhang, J. Huang, W. Zhang, Efficiently enhancing toughness of polylactic acid film through synergistic effect of bamboo charcoal and carbon fiber, Int. J. Biol. Macromol. 311 (2025) 143915, https://doi.org/10.1016/j.ijbiomac.2025.143915.
[34] M. Schilling, A. Ershov, R. Debastiani, K. Duan, K. Köble, S. Scherer, L. Lan, A. Rampf, T. Faragó, M. Zuber, A. Cecilia, S. Liu, C. Liu, T. Baumbach, J. Li, P.-C. Sui, R. Zeis, Bamboo charcoal as electrode material for vanadium redox flow batteries, Energy Adv. 3 (5) (2024) 997–1008, https://doi.org/10.1039/D4YA00166D.
[35] S. Qu, Q. Zhang, B. Liu, W. Li, Y. Wang, F. Li, J. Liu, Optimizing nozzle structure and parameters for continuous fiber prepreg filament 3D printing, Polymers 17 (8) (2025) 1014, https://doi.org/10.3390/polym17081014.
[36] R. Matsuzaki, M. Ueda, M. Namiki, T.-K. Jeong, H. Asahara, K. Horiguchi, T. Nakamura, A. Todoroki, Y. Hirano, Three-dimensional printing of continuous-fiber composites by in-nozzle impregnation, Sci. Rep. 6 (1) (2016) 23058, https://doi.org/10.1038/srep23058.

[37] K. Chen, L. Yu, Y. Cui, M. Jia, K. Pan, Optimization of printing parameters of 3D-printed continuous glass fiber reinforced polylactic acid composites, Thin-Walled Struct. 164 (2021) 107717, https://doi.org/10.1016/j.tws.2021.107717.
[38] A. le Duigou, A. Barbé, E. Guillou, M. Castro, 3D printing of continuous flax fibre reinforced biocomposites for structural applications, Mater. Des. 180 (2019) 107884, https://doi.org/10.1016/j.matdes.2019.107884.
[39] ASTM., ASTM D638-14: standard test method for tensile properties of plastics, ASTM, 2014.
[40] A.M. ASTM, ASTM D3039-standard test method for tensile properties of polymer matrix composite materials, Book ASTM D3039-standard test method for tensile properties of polymer matrix composite materials (ASTM International, 2017) 360 (2017).
[41] S. ASTM, Standard test methods for flexural properties of unreinforced and reinforced plastics and electrical insulating materials. ASTM D790, Annual book of ASTM Standards (1997).
[42] D. ASTM, 635; Standard Test Method for Rate of Burning and/or Extent and Time of Burning of Plastics in a Horizontal Position, ASTM International: West Conshohocken, PA, USA (2003).
[43] B. Du, X. Zhang, T. Wang, Y. He, M. Shen, T. Yu, Three-dimensional printable color-modulation and shape-programmable structures: an encryption key for image recognition electronic locks, Research 8 (2025), https://doi.org/10.34133/research.0666.
[44] G.M. Kanaginahal, V. Tambrallimath, M. Murthy, R.S. Mahale, A. Patil, S.Y. Pawar, P.P. Kakkamari, Flammability studies of natural fiber-reinforced polymer composites fabricated by additive manufacturing technology: a review, J. Instit. Eng. (India): Series D 105 (2) (2024) 1291–1303, https://doi.org/10.1007/s40033-023-00509-3.
[45] T. Zhang, Z. Wen, Y. Tan, P. Ekins, Circular economy strategies for the booming industrial pallet use in China, Sustainable Prod. Consumption 46 (2024) 244–255, https://doi.org/10.1016/j.spc.2024.02.028.